

The Giant Flare of 1998 August 27 from SGR 1900+14: II. Radiative Mechanism and Physical Constraints on the Source

C. Thompson^{1,3} and R.C. Duncan^{2,3}

Accepted for publication in the *Astrophysical Journal*
11 July 2001

ABSTRACT

The extraordinary 1998 August 27 giant flare places strong constraints on the physical properties of its source, SGR 1900+14. We make detailed comparisons of the published data with the magnetar model, which identifies the Soft Gamma Repeaters as neutron stars endowed with $\sim 10^{15}$ G magnetic fields. The giant flare evolved through three stages, whose radiative mechanisms we address in turn. The extreme peak luminosity $L > 10^6 L_{\text{edd}}$, hard spectrum, and rapid variability of the initial ~ 0.5 s spike emission all point to an expanding pair fireball with very low baryon contamination. We argue that this energy must have been deposited directly through shearing and reconnection of a magnetar-strength external magnetic field. Low-order torsional oscillations of the star fail to transmit energy rapidly enough to the exterior, if the surface field is much weaker. A triggering mechanism is proposed, whereby a helical distortion of the core magnetic field induces large-scale fracturing in the crust and a twisting deformation of the crust and exterior magnetic field. After the

¹Canadian Institute for Theoretical Astrophysics, 60 St. George St., Toronto, ON M5S 3H8

²University of Texas, Department of Astronomy & McDonald Observatory, Austin, TX 78712, USA

³Institute for Theoretical Physics, University of California, Santa Barbara, CA 93106, USA

initial spike (whose ~ 0.4 s duration can be related to the Alfvén-crossing time of the core), very hot ($T \lesssim 1$ MeV) plasma rich in electron-positron pairs remains confined close to the star on closed magnetic field lines. The envelope of the August 27 flare can be accurately fit, after ~ 40 s, by the contracting surface of such a “trapped fireball.” The form of this fit gives evidence that the temperature of the trapped pair plasma decreases outward from its center. We quantify the effects of direct neutrino-pair emission on the X-ray light curve, thereby deducing a lower bound $\mu_{min} \sim 1 \times 10^{32}$ G-cm³ to the magnetic moment of the confining field – comparable to the strongest fields measured in radio pulsars. The radiative flux during the intermediate ~ 40 s of the burst appears to exceed the trapped fireball fit. The lack of strong rotational modulation and intermediate hardness of this smooth tail are consistent with the emission from an extended pair corona, in which O-mode photons are heated by Compton scattering. This feature could represent residual seismic activity within the star, and accounts for ~ 10 percent of the total flare fluence. We consider in detail the critical luminosity, below which a stable balance can be maintained between heating and radiative cooling in a confined, magnetized pair plasma; but above which the confined plasma runs away to a trapped fireball in local thermodynamic equilibrium. The emergence of large-amplitude pulsations at ~ 40 s probably represents a transition to a pair-depleted photosphere whose main source of opacity is electrons (and ions) ablated from the heated neutron star surface. The best fit temperature of the black body component of the spectrum equilibrates at a value which agrees well with the regulating effect of photon splitting. The remarkable four-peaked substructure within each 5.16-s pulse, and the corresponding collimation of the X-ray flux, has a simple explanation based on the strong inequality between the scattering cross sections of the two photon polarization modes. The width of each X-ray ‘jet’ is directly related to the amount of matter advected outward by the high-cross section ordinary mode.

Subject Headings: gamma rays: bursts – stars: neutron – X-rays: stars

1. Introduction

On 1998 August 27, a giant flare of hard X-rays, lasting more than 5 minutes, was detected by Konus-Wind, *Ulysses* and BeppoSAX (Hurley et al. 1999a; Feroci et al. 1999; Mazets et al. 1999). It was only the second giant outburst detected from the Soft Gamma

Repeaters (SGRs), following nearly 20 years after the famous event on 1979 March 5 (Cline et al. 1982). The four or five known SGRs are identified by their frequent emission of much less energetic and shorter-duration bursts ($E \lesssim 10^{41}$ ergs, $\Delta t \lesssim 1$ s), whose peak luminosities reach nevertheless ten thousand times the Eddington luminosity. Statistically, the short bursts are similar to earthquakes and solar flares (Cheng et al. 1996; Gogus et al. 1999; Gogus et al. 2000).

SGR 1900+14, the source of the August 27 outburst, was first detected in 1979 (Mazets et al. 1979a), and became active again in 1992 (Kouveliotou et al. 1993) and in 1998 May (Kouveliotou et al. 1998a, Hurley et al. 1999b). ASCA and RXTE observations after the 1998 May activity episode revealed a periodicity of 5.16 s in the quiescent X-ray emission with period derivative $\sim 1 \times 10^{-10} \text{ s s}^{-1}$ (Hurley et al. 1999c, Kouveliotou et al. 1999; Woods et al. 1999). A rapid spindown $\dot{P} \sim 10^{-10} \text{ s s}^{-1}$ and 7.47 spin period was also measured for SGR 1806-20 (Kouveliotou et al. 1998b) These apparent rotation periods are similar to that of SGR 0526-66, which displayed an 8 s periodicity during the giant flare of 1979 March 5 (Mazets et al. 1979b, Barat et al. 1979). At least two of the SGRs are associated with supernova remnants (SNRs) and/or radio plerions (Hurley 2000). However, the recently-verified position of SGR 1900+14 (Vasisht et al. 1994; Hurley et al. 1999d; Murakami et al. 1999; Frail, Kulkarni & Bloom 1999) lies just outside the edge of G43.8+0.6, a $\lesssim 10^4$ -year-old galactic SNR. It is plausible that SGR 1900+14 was born in this SNR, since the *other* known giant flare source, SGR 0526-66, has a position inside but near the the edge of a $\lesssim 10^4$ -year-old SNR in the Large Magellanic Cloud (Cline et al. 1982).

The SGRs have been identified with *magnetars* (Duncan & Thompson 1992, “DT92”): neutron stars in which magnetism rather than rotation or accretion is the dominant source of energy for radiative and particle emissions. The hypothesized $\sim 10^{14} - 10^{15}$ G magnetic fields of these stars are consistent with many observed SGR properties, including the very high energies and hyper-Eddington luminosities of the outbursts, the long spin periods, rapid spindown rates, strong X-ray emissions in the quiescent state, and the young ages of active stars (DT92; Paczyński 1992; Thompson & Duncan 1995, “TD95”; Thompson & Duncan 1996, “TD96”; Thompson et al. 2000).

A recent joint paper (Feroci et al. 2000, hereafter Paper I) analyzed the Ulysses and BeppoSAX observations of the August 27 giant flare, and drew some conclusions about the underlying physics of the event. The intense, hard spike of gamma-rays during the first 0.4 second was identified with a freely expanding pair fireball, which requires a very clean energy source. We found that the subsequent rotation-cycle averaged flux diminished monotonically, or nearly so. This strongly suggests that most of the burst energy was

released at early times, near the beginning of the flare, and that the energy which did not escape promptly during the initial hard spike ($t \lesssim 0.4$ s) was retained by the star as a residue, to leak away on longer timescales.

In principle, such an energy residue could take several forms. Some energy could be in the form of an optically-thick pair-photon plasma contained in the magnetosphere by closed magnetic field lines (TD95), which we will call a “trapped fireball.” Additional energy could be stored within the star itself in the form of a internal oscillations, including a torsional Alfvén mode in the liquid core; or a standing shear wave in the neutron star crust (McDermott, Van Horn, & Hansen 1988; Duncan 1998). Thus, observations of the flare and its aftermath give clues about the way in which the energy residue is partitioned among various components.

In this paper, we begin by discussing the general issue of SGR energy budgets in §2, estimating the minimum magnetic field needed to power both the bursting and quiescent emission of the SGRs. Then, in §3 we consider the physical states of magnetars on the threshold of a giant flare, with a particular focus on how and where the energy that powers the flare is stored, and how its catastrophic release may be triggered. Our favored model involves a wound-up magnetic field that is pinned by the neutron star crust.

With this background information developed, we then begin to consider successive stages of the 1998 August 27 flare. In Paper I we showed that the envelope of the August 27 light curve, smoothed over the 5.16-s rotation period during the interval from 40 to 400 s after the onset of the flare, is well-fit by a mathematical curve describing the cooling of a zone of very hot plasma composed of γ -rays and electron-positron pairs. Such a “trapped fireball” cools through the formation of a sharp temperature gradient inside its outer boundary, which propagates inward in a “cooling wave” (TD95). In particular, this model matches the rapid, late decline in the X-ray flux at ~ 400 s after the flare onset. The observed terminal drop in the X-ray flux is does not appear to be consistent with models in which the emissions are powered by cooling surface hotspots or by incremental internal mode damping. In §4 of this paper, we relate the measured slope of the lightcurve to the internal properties of the fireball and study the effects of neutrino cooling on the trapped fireball.

The extreme properties of the giant flare lead to stringent bounds on its magnetic field (DT92; Paczyński 1992; TD95). In §5.1 we use the condition that the trapped fireball energy must remain confined by the magnetic field to derive lower bounds on the star’s magnetic dipole moment. We generalize this argument by considering deviations from centered-dipole geometry, which imply a lower magnetic moment for a fixed fireball energy. We show that the lower bound on the magnetic moment cannot be significantly weakened

without raising the temperature of the confined plasma sufficiently that almost all its energy is lost to neutrino pair emission, rather than X-rays.

Then, in §5.2, we show how the extremely high peak luminosity of the hard spike (more than a million times the Eddington luminosity of a neutron star) points to the presence of magnetic fields stronger than $\sim 10^{14}$ G. Because the magnetic field lines are tied to material of a very high density, a sudden release of elastic stresses in the deep crust occurs only gradually compared with the time $\sim R_{\text{NS}}/c \sim 3 \times 10^{-4}$ s for an Alfvén-like excitation to cross the magnetosphere. As a result, the high measured luminosity is consistent with external shearing and reconnection of the external field, but only if the flux density exceeds $\sim 10^{14}$ G. For essentially the same reason, an internal shear wave cannot transmit energy to the magnetosphere at $\sim 10^6 L_{\text{edd}}$ in weaker magnetic fields. We contrast our results with the previous suggestion that an internal p -mode or f -mode excitation of a neutron star could induce strong shock heating of the surface layers and electromagnetic damping in the magnetosphere (Ramaty et al. 1980; Lindblom & Detweiler 1983), even if the surface magnetic field were only $\sim 10^{12}$ G. We explain how two basic assumptions of this model – that the surface layers would be shock heated, and that external Alfvén modes could be excited with $\delta B/B \sim 1$ by an internal oscillation – are very likely incorrect. Indeed, Blaes et al. (1989) have shown that internal shear modes have a much stronger coupling to the magnetosphere than do p - and f -modes.

Some aspects of giant flare emission spectra and spectral evolution are elucidated in §6. In particular, we consider the hard spectrum of the initial spike in §6.1, and argue that the hardest γ -ray photons must be generated at more than $\sim 10^{10}$ cm from the star, due to the same limitations of pair opacity that arise in models of cosmological gamma-ray bursts. The equilibrium temperature of the pulsating soft tail fitted in Paper I is shown in §6.2 to agree with the calculation in TD95 of the freeze-out of photon splitting in a strongly-magnetized scattering atmosphere.

The first ~ 40 seconds of the August 27 flare showed only mild and irregular pulsations at the 5.16 spin period, with a higher flux and harder spectrum than the remainder of the burst. This excess emission over the predictions of the trapped fireball curve amounts to 20% of the burst fluence (Paper I). In §7, we interpret this 40-s “smooth tail” as the signature of a transient and extended pair corona, powered by residual creep of the neutron star crust following the principal disruption. In particular, we consider the thermodynamic stability of a strongly magnetic pair atmosphere, in which X-ray photons are subject simultaneously to Compton scattering and splitting. We show that this corona is thermally unstable if the pairs are heated at a rate exceeding $\sim 10^{42}$ ergs s^{-1} within a volume $(10 \text{ km})^3$.

Around ~ 40 s following the flare trigger, large-amplitude modulations appeared in the light curve with a remarkable four-peaked structure. These peaks were maintained with a 5.16-s period (equal to the spin period measured in quiescence) during most of the rest of the event. In §8, we examine in more detail the proposal of TD95 that the cooling X-ray flux from a trapped fireball in a super-QED magnetic field will be collimated along (partly) open magnetic field lines. In this picture, the complicated pulse shape provides a template of higher multipoles in the neutron star’s surface magnetic field.

Finally, in §9 we summarize all of the evidence, based on the study of giant flares and their aftermaths, for magnetic fields $\gtrsim 10 B_{\text{QED}} = 4.4 \times 10^{14}$ G in SGRs, and the main new implications of this work for the physics of magnetars.

In what follows, we use the convenient reference field

$$B_{\text{QED}} = \frac{m_e^2 c^3}{e \hbar} = 4.4 \times 10^{13} \text{ G}, \quad (1)$$

at which the non-relativistic Landau energy $\hbar e B / m_e c$ formally becomes equal to the electron rest energy $m_e c^2$.

2. Strong Magnetic Fields in the SGR Sources

The electromagnetic output of an SGR source consists of both hard X-ray outbursts and the persistent X-ray emission. The core of the star may release an even larger energy in the form of thermal neutrinos, over its active lifetime (TD96). We now estimate the minimal magnetic field needed to power the observed activity. The close affinity between the SGR and AXP sources (some of which have variable persistent X-ray output even in the absence of bursts) indicates that an SGR can dissipate magnetic energy in two distinct modes: first, in an episodic manner through brittle fracturing of the crust; and, second, through a more plastic deformation of the star (TD96).

2.1. Energetic Requirements

The association of several magnetar candidates (three AXPs and at least two SGRs) with young supernova remnants, $t_{\text{SNR}} \lesssim 10^4$ yr (Hurley 2000), combined with the short spindown times of these stars, suggests an active lifetime of order of magnitude $\sim 10^4$ yr. Two giant flares have been detected from four verified, active SGR sources within the last 30 years. The implied flaring rate is $\sim 10^{-2}$ per year per source, suggesting a total number of giant flares $N_{\text{giant}} \sim 10^2$ from each source during its active lifetime $\sim 10^4$ yr. Since the

measured X-ray and gamma ray output of the 1979 March 5 and 1998 August 27 flares exceed $\sim 5 \times 10^{44}$ ergs and $\sim 1 \times 10^{44}$ ergs respectively, the total flare energy released per source is

$$E_{\text{flare}} \gtrsim 3 \times 10^{46} \left(\frac{\dot{N}_{\text{giant}}}{10^{-2} \text{ yr}^{-1}} \right) \left(\frac{t_{\text{active}}}{10^4 \text{ yr}} \right) \text{ ergs} \quad (2)$$

The persistent X-ray luminosity of SGR 0526-66 is $\sim 10^{36}$ ergs s^{-1} (Kulkarni et al. 2000) and is approximately 10^{35} ergs s^{-1} for SGR 1806-20 and SGR 1900+14 during periods of quiescence (Murakami et al. 1994; Woods et al. 2000). The net energy released in persistent X-ray emission can therefore be estimated as

$$E_X \sim L_X t_{\text{active}} = 3 \times 10^{46} \left(\frac{L_X}{10^{35} \text{ ergs s}^{-1}} \right) \left(\frac{t_{\text{active}}}{10^4 \text{ yr}} \right) \text{ ergs} \quad (3)$$

over the active lifetime. Thus, the observed electromagnetic output of an SGR is fairly evenly divided between flares and its highly non-thermal persistent emission. The observation of a transient enhancement in the persistent output of SGR 1900+14 following the August 27 flare (Woods et al. 2000) establishes a close physical connection between the two phenomena. This enhanced emission has been ascribed to persistent currents excited by non-potential deformations of the external magnetic field, caused by the shifting positions of magnetic footpoints which are anchored to an evolving crust (Thompson et al. 2000).

It is possible that significant power is emitted at wavelengths intermediate between X-rays and optical in sources such as SGR 0526-66 with soft power-law spectral components (Kulkarni et al. 2000). Such intermediate wavelengths are not observable in known galactic magnetar candidates because of the opacity of the intervening interstellar medium. In the case of the low-extinction LMC source SGR 0526-66, spectral measurements at $\lesssim 0.5$ keV are not yet available. For sources with hard power-law spectra (photon index ~ -2 or less steep) extending to low energies, the correction factor to eqn. (3) would be of order unity only.

It is instructive to compare E_{flare} with the energy detected in ordinary, short-duration SGR bursts. These events are distributed over a wide range of energies $\sim 10^{37} - 10^{41}$ ergs, with a power-law $dN/dE \sim E^{-5/3}$, so that the integrated energy is dominated by large events (Cheng et al. 1996; Gogus et al. 2000). Nonetheless, many fewer than $\sim 10^3$ events with energies $\sim 10^{41}$ ergs have been detected during the same time that two giant flares have been observed. This suggests that the time-averaged output in short bursts is lower than either in the giant flares or persistent emission.

2.2. Magnetic Field Strength

For the reasons just described, the persistent and bursting output of an SGR source appear to draw from the same energy reservoir, which at minimum is $E_{\min} \sim 10^{47}$ ergs per source. The present rotational energy is much smaller, $\frac{1}{2}I\Omega^2 = 5 \times 10^{44}(P/6 \text{ s})^{-2}$ ergs. It has been suggested that the SGR/AXP sources were born spinning much more rapidly, $P \lesssim 3$ msec, and that a fraction of this initial rotational energy was converted to a strong magnetic field through an $\alpha - \Omega$ dynamo in the convective proto-neutron star (DT92). This magnetic field would then provide a reservoir of energy for later bursting activity. An alternative form of potential energy for bursting activity involves an elastic deformation of the crust, resulting from the changing figure of the rotating star as its rate of spin decreases (e.g Baym et al. 1969). However, the maximum elastic energy which can be stored by the crustal lattice is only $\frac{1}{2}M_{crust} V_{\mu}^2 \psi_{cr}^2 = 1 \times 10^{42} (V_{\mu}/10^8 \text{ cm s}^{-1})^2 (M_{crust}/10^{-2} M_{\odot}) (\psi_{cr}/0.003)^2$ ergs (eq. [11]), too small to power a single giant flare except under the most optimistic assumptions about the breaking strain ψ_{cr} . (Here V_{μ} is the shear wave velocity, which is nearly independent of density in the deep crust.) Even in sources which have not emitted giant flares, the elastic energy would need to be replenished on a timescale short compared with the spindown age; but the present rotational energy is insufficient for that purpose.

Accretion power is not a promising energy source for the hard-spectrum, hyper-Eddington SGR outbursts, nor for persistent X-ray emission from SGRs. The observation of persistent emission from SGR 1900+14 within 1000 s of the 27 August 1997 giant flare (Woods et al. 2000) seems inconsistent with accretion-powered scenarios, because even $\sim 10^{-3}$ of the radiative momentum of the flare would excavate the accretion flow and suppress accretion for a much longer time period (Thompson et al. 2000). Accretion models also have difficulty accomodating the power-law distribution of energies of ordinary SGR bursts, and the lognormal distribution of waiting times between bursts (Cheng et al. 1996; Gogus et al. 1999, 2000). Recent HST bounds on the optical emission from SGR 0525-66 set an upper limit of $L_{\text{opt}}/L_X \sim 10^{-3}$ for reprocessed optical emission from an accretion disk (Kaplan et al. 2001), an order of magnitude less than is expected from an accretion disk (Perna, Hernquist, & Narayan 2000). Optical and infrared observations also exclude the simplest disk models of the Anomalous X-ray Pulsars [AXPs] (Hulleman et al. 2000a; Hulleman, van Kerkwijk & Kulkarni 2000), which resemble SGRs in inactive phases. In particular, 4U 0142+61 has a possible optical counterpart with a much redder spectrum than is typical of LMXBs (Hulleman et al. 2000b). Some other arguments against accretion-powered models of SGRs are given in §7.3 of TD95.

Magnetic energy, on the other hand, can be a good “clean” power source for both hyper-Eddington bursts and the hard fireball component of the giant flares (DT92;

Paczynski 1992; TD95). A first estimate of the minimum magnetic field is obtained by averaging over the volume of the star,

$$B_{\min} = \left(\frac{6E_{\min}}{\epsilon_B R_{\text{NS}}^3} \right)^{1/2} = 8 \times 10^{14} \epsilon_B^{-1/2} \left(\frac{E_{\min}}{10^{47} \text{ ergs}} \right)^{1/2} \left(\frac{R_{\text{NS}}}{10 \text{ km}} \right)^{-3/2} \text{ G}. \quad (4)$$

Here ϵ_B denotes the efficiency of conversion of magnetic energy to X-rays.

If the protons in the stellar interior form a Type II superconductor, then the magnetic field is confined to fluxoids with flux density comparable to the lower critical field $B_{c1} \sim 2 \times 10^{15} \text{ G}$ (e.g. Easson & Pethick 1979). The mean field in the core is related to B_{c1} by the volume-filling fraction f of the fluxoids, $\langle B \rangle = B_{c1} f$, and the magnetic energy per unit volume is $B_{c1}^2 f / 8\pi = \langle B \rangle B_{c1} / 8\pi$. When the mean field $\langle B \rangle < B_{c1}$ (that is, when the efficiency of conversion of core magnetic energy to X-rays is less than ~ 10 percent) expression (4) decreases by a factor $\sim \epsilon_B^{-1/2} (B_{\min} / B_{c1})$. Otherwise, the minimum field is not modified to first order by proton superconductivity.

If $\epsilon_B \sim 1$, expression (4) is similar to the dipolar magnetic fields that are inferred from the rapid spindown of the SGRs (Kouveliotou et al. 1998b, 1999) and AXPs (TD96). However, the total magnetic energy of the star is almost certainly larger than its minimum value, because the currents that support the field flow through very highly conducting material and cannot entirely dissipate. Very strong core magnetic fields also seem to be required by models of core ambipolar diffusion which include the accelerating effects of core heating by the decaying field (TD96; Heyl & Kulkarni 1998). Only fields stronger than $\sim 10^2 B_{\text{QED}} \sim 5 \times 10^{15} \text{ G}$ are transported over a distance $\sim 10 \text{ km}$ in times less than $\sim 10^4 \text{ yr}$, typical of SGR active lifetimes.

The magnetic flux density inside an SGR/AXP source probably lies below the upper critical field where proton superconductivity is fully quenched, $B_{c2} \sim 10^{17} \text{ G}$. Nonetheless, the extended magnetic sheaths of the fluxoids are very densely packed in fields $\gtrsim B_{c1}$. As a result, field transport driven by collective effects such as vortex-line sweeping (Ruderman 1991) is probably suppressed in slowly-rotating magnetars.

Several lines of evidence suggest that SGR bursts and flares are powered by *internal* magnetic stresses acting on the deep crust and core. The hard initial γ -ray spikes observed in the two giant flares had durations $\sim 0.2 - 0.5 \text{ s}$. This is comparable to the time for a $\gtrsim 10^{15} \text{ G}$ magnetic field to rearrange material in the dense stellar core (TD95), but it is much longer than the timescales for global rearrangements of either the magnetosphere ($\sim R_{\text{NS}}/c \sim 0.03 \text{ ms}$) or the stellar crust ($R_{\text{NS}}/V_{\mu} \sim 10 \text{ ms}$; see also eqs. [8] and [31] below). Furthermore, the cumulative fluence of short SGR bursts is observed to rise linearly with time during periods of activity (Palmer 1999). This “relaxation system” behavior

indicates that a reservoir of energy is steadily loaded and undergoes stochastic, catastrophic relaxations. For example, such a reservoir could encompass a fraction of the star’s surface, steadily dragged from below by the tension of field lines experiencing core ambipolar diffusion (TD96). This model is roughly analagous to what happens in earthquakes, where relaxation-system behavior driven by crustal plate motion is also found (see Palmer 1999; Gogus et al. 1999, 2000, and references therein).

The magnetic field geometry of an SGR/AXP source almost certainly involves higher multipoles (for which the August 27 lightcurve provides clear evidence: Paper I; §8 below); and quite plausibly a strong toroidal field component in the deep crust and core, as would result from post-collapse α - Ω dynamo action (DT92; Thompson & Duncan 1993, hereafter TD93). This suggests that the magnetic energy of a magnetar is dominated by the internal field, with a probable value

$$E_{\text{magnetic}} = 3 \times 10^{48} f_B \left(\frac{B_{\text{internal}}}{100 B_{\text{QED}}} \right)^2 \text{ ergs}, \quad (5)$$

where f_B is the fraction of the star’s volume filled by the strong field.

Comparisons of eqs. (2), (3) and (5) indicate that *only a fraction $\epsilon_B \sim 0.03/f_B$ of the star’s magnetic energy must be dissipated in the form of X-rays and gamma-rays to power all observed SGR activity*. Indeed, most of the core field energy is probably lost to thermal neutrinos or ultimately remains trapped in the core when the epoch of SGR activity ends.

3. Giant Flare Mechanism

The crust of a magnetar is subjected to strong, evolving magnetic stresses. The star must initially relax to an equilibrium configuration before the crust forms (but after it becomes compositionally stratified: Lattimer & Mazurek 1981; Reisenegger & Goldreich 1992). Observations of magnetic white dwarfs prove that static, magnetized equilibrium states exist even in the absence of any rigidity due to solidification. After the neutron star crust forms, the crust, core and field evolve through a sequence of equilibrium states in which magnetic stresses are balanced by both hydrostatic forces and elastic stresses in the crust. The star evolves via the very slow transport of the field through the core (by ambipolar diffusion) and the crust (by Hall drift) (Goldreich & Reisenegger 1992; TD96). Because the crust has a finite shear strength, these equilibria are punctuated by starquakes whenever the crust is strained past its breaking point.

We now review the forms in which potential energy can be stored inside a magnetar, and how some of this stored energy can be transferred to the external magnetic field,

to heat, and to internal torsional and standing shear waves. This suggests a candidate mechanism for triggering giant flares like the March 5 and August 27 events.

3.1. Stored Elastic and Magnetic Energy

A Soft Gamma Repeater stores a certain amount of potential energy which can drive rapid rearrangements of the external magnetic field, thereby triggering bright X-ray outbursts. This potential energy can be divided into an elastic component in the crust, and magnetic components in the crust, core and magnetosphere. The portion of the magnetic energy which is available to do mechanical work can easily be estimated, in a situation where the accumulation and release of stress is caused by pinning of the internal magnetic field by the crust.

The elastic energy corresponding to a static shear strain ψ can be well approximated by⁴

$$E_{\text{elas}} = \frac{1}{2} \int d\Omega \int_{R_{\text{NS}} - \Delta R_0}^{R_{\text{NS}}} \mu \psi^2 r^2 dr = \frac{1}{2} \left(\frac{\gamma}{\gamma - 0.2} \right) \langle \psi^2 \rangle M_{\text{Coulomb}} V_{\mu 0}^2. \quad (6)$$

In this expression, the shear modulus is⁵

$$\mu = 1.1 \times 10^{30} \rho_{14}^{0.8} \text{ ergs cm}^{-3}, \quad (7)$$

and the shear wave speed,

$$V_{\mu} = (\mu/\rho)^{1/2} = 1.0 \times 10^3 \rho_{14}^{-0.1} \text{ km s}^{-1}, \quad (8)$$

depends weakly on the density $\rho = \rho_{14} \times 10^{14} \text{ g cm}^{-3}$ at densities above neutron drip (Baym & Pines 1971; Strohmayer et al. 1991, Fig. 3). The integral (6) extends from the base of the Coulomb lattice at a depth ΔR_0 (density ρ_0 and shear wave speed $V_{\mu 0}$). It has been evaluated using the equation of hydrostatic equilibrium $dP/dr = -\rho g$, and fitting a power-law relation between the pressure and density profiles, $P(r) \propto [\rho(r)]^{\gamma}$. In particular, the equation of state of Negele & Vautherin (1973) gives $\gamma \simeq 1.47$ and

$$P(\rho) = 3.75 \times 10^{32} \rho_{14}^{1.47} \text{ ergs cm}^{-3} \quad (9)$$

⁴This generalizes the expression given in Duncan (1998), to allow for a variable position (density) at the base of the rigid Coulomb lattice.

⁵The neutron star crust is here approximated as a body-centered cubic (bcc) Coulomb lattice (Ogata & Ichimaru 1990; Strohmayer et al. 1991), with ionic mass and charge determined by a power-law fit to the equation of state of Negele & Vautherin (1973).

above a density 3.6×10^{12} gm cm $^{-3}$. The mass within the Coulomb lattice

$$M_{\text{Coulomb}} = \int_{R_{\text{NS}} - \Delta R_0}^{R_{\text{NS}}} \rho(r) 4\pi r^2 dr = \frac{4\pi R_{\text{NS}}^2 P(\rho_0)}{g(R_{\text{NS}})} \quad (10)$$

excludes a transition layer at its base where the nuclei have strongly aspherical shapes, forming rod-like and plane-like structures, with bulk elastic properties resembling those of a liquid crystal (Pethick & Potekhin 1998). Normalizing the base density ρ_0 to a fraction 0.6 of the nuclear saturation density $\rho_{\text{sat}} = 2.7 \times 10^{14}$ g cm $^{-3}$, expressions (6) and (10) become

$$E_{\text{elas}} = 1.7 \times 10^{43} \Lambda^{-1} \left(\frac{\langle \psi^2 \rangle}{(10^{-2})^2} \right) \left(\frac{\rho_0}{0.6 \rho_{\text{sat}}} \right)^{1.27} \left(\frac{R_{\text{NS}}}{10 \text{ km}} \right)^4 \left(\frac{M_{\text{NS}}}{1.4 M_{\odot}} \right)^{-1} \text{ ergs}, \quad (11)$$

and

$$M_{\text{Coulomb}} = 0.025 \Lambda^{-1} \left(\frac{\rho_0}{0.6 \rho_{\text{sat}}} \right)^{1.47} \left(\frac{R_{\text{NS}}}{10 \text{ km}} \right)^4 \left(\frac{M_{\text{NS}}}{1.4 M_{\odot}} \right)^{-1} M_{\odot}. \quad (12)$$

The scaling with stellar radius R_{NS} and mass M_{NS} assumes a fixed equation of state, and arises because the hydrostatic pressure $P(\rho_0) \sim [g(R_{\text{NS}})M_{\text{Coulomb}}/4\pi R_{\text{NS}}^2]$ at the base of the crust is fixed by the nuclear interactions (Lorenz, Ravenhall, & Pethick 1993). The factor $\Lambda^{-1} = 1 - 2GM_{\text{NS}}/R_{\text{NS}}c^2 \simeq 0.6 - 0.7$ is a relativistic correction to the surface gravity, $g(R_{\text{NS}}) = GM_{\text{NS}}\Lambda/R_{\text{NS}}^2$.

Comparing expression (11) with the energy of the 1979 March 5th event, $E_{\text{March5}} \approx 5 \times 10^{44}$ ergs, it is clear that even for the optimistic case $\psi_{\text{cr}} \sim 10^{-2}$, giant flares cannot be powered by pure elastic energy stored within the crust of a neutron star. Furthermore, it is often assumed that ψ_{cr} is one or more orders of magnitude less than the value $\sim 10^{-2}$ appropriate for a perfect bcc lattice, since lattice imperfections inevitably weaken the solid (e.g. Ruderman 1991). But the critical strain ψ_{cr} for a large-scale yield in the gravitationally-stratified crust of a neutron star is actually highly uncertain. Any motion of the crust over a scale of kilometers is severely constrained, because the hydrostatic pressure in the deep crust exceeds the shear modulus by a factor $\sim 10^3$. Degeneracy pressure and buoyancy forces provide strong resistance to bulk compressions and to vertical displacements within the crust. Observations of giant flares probe the behavior of Coulomb solids in a regime of high pressure and large applied stress that has no direct experimental analogs.

It should be emphasized at this point the magnetic field which stresses the crust can store much more potential energy than the Coulomb lattice itself. Within the crust, the force balance

$$\frac{B\delta B}{4\pi} \sim \psi\mu \quad (13)$$

implies that

$$\frac{(\delta B)^2/8\pi}{\frac{1}{2}\psi^2\mu} = \left(\frac{B_\mu}{B_{\text{crust}}}\right)^2. \quad (14)$$

when $B < B_\mu$. Here

$$B_\mu \equiv (4\pi\mu)^{1/2} = 4 \times 10^{15} \rho_{14}^{0.4} \text{ G} \quad (15)$$

is a characteristic field above which the crust tends to respond plastically to applied magnetic stresses. For $B > B_\mu$, the equilibrium condition (13) requires that the strain angle of the Coulomb solid exceed $\delta B/B$, even while the field remains tied to the highly conducting solid (TD95). In weaker fields $B < B_\mu$, the field stores more potential energy than the lattice. This field energy might be tapped in short SGR bursts, which would require that the crustal material undergoes abrupt plastic deformation. However, a very weak field $B \ll B_\mu$ does not have the strength to move the crust, even as the ratio in eq. (14) formally becomes enormous. For example, when

$$B < B_{\text{frac}} = \psi_{\text{cr}}^{1/2} B_\mu = 1 \times 10^{14} \left(\frac{\psi_{\text{cr}}}{10^{-3}}\right)^{1/2} \rho_{14}^{0.4} \text{ G} \quad (16)$$

magnetic stresses within the crust are too weak to induce any yields or fractures.

3.1.1. A Globally Twisted Magnetic Field

The giant flares involve a large disturbance which probably is driven by a rearrangement of magnetic field in the deep crust and core (TD95). It is important therefore to consider the case in which the crust is stressed *from below* by the evolving magnetic field in the liquid interior of the neutron star. A related configuration has been considered by Ruderman (1991), in a situation where mean core field is much weaker than 10^{15} G, and its transport is driven by spindown. As we now show, a factor similar to (14) relates the available magnetic energy *stored in the core* to the elastic energy built up in the crust. The flux density B which enters this relation turns out to be the poloidal field which threads the core-crust boundary.

At least two lines of argument suggest that the interior magnetic field of the SGR and AXP sources is strongly wound, with a large toroidal component: first, their association with neutron stars that were formed with rapid rotation and strong differential rotation (DT92); and, second, their non-thermal and transient persistent X-ray emission (Thompson, Lyutikov, & Kulkarni 2001). We therefore focus on a cylindrically symmetric star with a uniform poloidal field $B_z < B_\mu$ in its interior (Fig. 1). In the core, the evolving field is assumed to be twisted about the magnetic dipole axis (the axis of symmetry), generating

a field component B_ϕ . In static equilibrium, before the critical point is reached, the stress $B_z B_\phi / 4\pi$ applied to the lower base of the crust is balanced by an elastic stress $\sigma_{\varpi\phi} = \mu\varpi(d\phi/d\varpi) = \mu\psi$ within the crust, so that

$$\frac{B_z B_\phi}{4\pi} = \frac{\Delta R_\mu}{\varpi} \frac{d}{d\varpi} (\varpi \sigma_{\varpi\phi}). \quad (17)$$

Here, ΔR_μ is the stress-averaged depth of the crust,

$$\Delta R_\mu = \frac{1}{\mu(\rho_0)} \int_0^{\rho_0} \left(\frac{dP}{d\rho} \right) \frac{\mu(\rho)}{\rho g} d\rho = 0.27 \Lambda^{-1} \left(\frac{\rho_0}{0.6 \rho_{\text{sat}}} \right)^{0.47} \left(\frac{R_{\text{NS}}}{10 \text{ km}} \right)^2 \left(\frac{M}{1.4 M_\odot} \right)^{-1} \text{ km} \quad (18)$$

(Duncan 1998). Expression (17) remains a good approximation as long as the spherical curvature of the neutron star crust can be neglected; that is, at cylindrical radius $\varpi \lesssim \frac{1}{2} R_{\text{NS}}$. Integrating out from the axis of symmetry ($\varpi = 0$), and assuming the power-law dependence

$$\varpi B_\phi \propto \psi \propto \varpi^\alpha, \quad (19)$$

equation (17) implies $B_z B_\phi / 4\pi = (1 + \alpha)(\Delta R_\mu / \varpi) \mu \psi$. The parameter $\alpha = 2$ corresponds to a twist angle that is independent of ϖ ; whereas $\alpha = 0$ corresponds to a current that is localized on the symmetry axis.

Notice that the equilibrium strain $\psi(\varpi)$ increases away from the axis of symmetry for $\alpha > 0$ (eq. 19). This means that the crust can be expected to break first at a radius ϖ_{frac} where

$$\psi(\varpi_{\text{frac}}) \sim \psi_{\text{cr}}, \quad (20)$$

the critical strain angle. If the strain increases monotonically with time, this means that fracture first occurs at $\varpi_{\text{frac}} \sim (\frac{1}{2} - 1) R_{\text{NS}}$.

The energy stored in the twisted magnetic field is

$$\delta E_{\text{mag}} = (2R_{\text{NS}} \cdot \pi\varpi^2) \frac{B_\phi^2}{8\pi} = \pi(\alpha + 1)^2 \psi^2(\varpi) \mu \left(\frac{B_\mu}{B_z} \right)^2 (\Delta R_\mu)^2 R_{\text{NS}}, \quad (21)$$

per logarithm of cylindrical radius ϖ . This can be expressed as

$$\delta E_{\text{mag}} = 4 \times 10^{44} \left(\frac{\psi^2(\varpi)}{(10^{-2})^2} \right) \left(\frac{B_z}{10 B_{\text{QED}}} \right)^{-2} \left(\frac{\rho_0}{0.6 \rho_{\text{sat}}} \right)^{1.6} \left(\frac{\Delta R_\mu}{0.3 \text{ km}} \right)^2 \text{ ergs} \quad (22)$$

for $\alpha = 2$. It is also worth comparing eq. (22) with the crustal strain energy. The available magnetic energy in the core is the larger by a factor

$$\frac{(B_\phi^2/8\pi) R_{\text{NS}} \cdot \pi\varpi^2}{(\frac{1}{2}\psi^2\mu) \Delta R_\mu \cdot \pi\varpi^2} = \left(\frac{B_\mu}{B_z} \right)^2 \frac{(1 + \alpha)^2 R_{\text{NS}} \Delta R_\mu}{\varpi^2}. \quad (23)$$

This expression exceeds (14) by a geometrical factor, which works out to $\sim 2(\varpi/\frac{1}{3}R_{\text{NS}})^{-2}$ in the case of a uniformly twisted field ($\alpha = 2$). Thus, *in the giant flare the main role of the crust is to serve as a gate to facilitate the storage and episodic release of interior magnetic energy, not as a reservoir of energy itself.*

In this toy model, the available magnetic energy (22) suffices to power a single giant flare, if $\psi_{\text{cr}} \sim 10^{-2}$. This yield strain is larger than usually adopted for neutron star crusts (e.g. Ruderman 1991), but it may not be unreasonable given the large hydrostatic pressure and near incompressibility of the crustal material. The required value of ψ_{cr} is reduced if the poloidal current flowing through the star varies in sign, with multiple interior zones in which the toroidal field has a magnitude comparable to its limiting value (13). Then the winding energy (22) is multiplied by the number of zones N , and ψ_{cr} decreases by a factor $N^{-1/2}$. However, the hydromagnetic stability of such a configuration is not certain.

Although the energy that can be released in one giant flare is limited by the shear strength of the crust, this simple model significantly underestimates the total energy that can be released over successive flares. In addition, in this simplified geometry the twist of the core field must be assumed to increase with time to reach a point of instability. Both apparent difficulties can be addressed by noting that the stratification of the core allows the field to retain a significantly *larger* twist than can be dissipated in a single flare.

Consider an electrically conducting medium that is stratified along planes, which run perpendicular to the direction of gravity. This stratification is assumed to be stable to convection, in the sense that internal g-modes have real frequencies. The gradient of electron fraction in the core of a neutron star provides just such a stable stratification (Reisenegger & Goldreich 1992). A cylindrical bundle of magnetic flux threads the medium, tilted at an angle α with respect to gravity (Fig. 2a). We assume that the magnetic field is weak, in the sense that the fluid motions driven by the $\mathbf{J} \times \mathbf{B}$ force lie almost parallel to the equipotential surfaces. If $\alpha = 0$, then the flux bundle can unwind entirely through such constrained motions, as long as its ends are not pinned. By contrast, if $\alpha = \pi/2$ and the flux bundle runs perpendicular to gravity, then any motion of the field and entrained conducting fluid which reduces the twist must involve the motion of fluid elements *across* the equipotential surfaces. This means (Fig. 2b) that a localized twist will not be able to spread out along the flux bundle – even if the ends of the bundle are not pinned by external forces.

For an arbitrary value of α , it is clear that any initial twist will be able to relax only partially. In particular, if the field is strongly twisted, $B_\phi \gtrsim B_z/\tan\alpha$, then the flux bundle will relax to a magnetostatic equilibrium without B_ϕ/B_z being significantly reduced in magnitude. To see this, consider a cylindrical bundle of flux which is unpinned at either

end. Coordinate z runs along the axis of the flux bundle, and gravity lies in the plane $\phi = 0$. The twisted bundle is allowed to deform from this initial condition, subject to the constraint that the component of the velocity parallel to gravity vanishes,

$$V_z \cos \alpha - V_\phi \sin \alpha \cos \phi = 0. \quad (24)$$

(We neglect deviations from cylindrical symmetry, so that in this coordinate system the radial components B_R and V_R both vanish. In effect, the flux bundle and the stratified medium are assumed to be confined with an infinitely rigid cylindrical shell.) The induction equation then becomes

$$\frac{\partial B_\phi}{\partial t} = \frac{\partial}{\partial z} (V_\phi B_z - V_z B_\phi) = \frac{\partial}{\partial z} [V_\phi (B_z - B_\phi \tan \alpha \sin \phi)]. \quad (25)$$

One sees that if $B_\phi \gg B_z / \tan \alpha$, then a rotation of surfaces of constant z cannot reduce B_ϕ by more than a factor of two, because the second term in the induction equation is not symmetric about the axis of the cylinder.

Slower transport processes such as ambipolar diffusion can change α over timescales much longer than the hydromagnetic time R_{NS}/V_{Az} . In this manner, elastic stresses can build up if the flux bundle is tied to a rigid medium (e.g. the neutron star crust).

3.2. Release of Stored Magnetic Energy

The two giant flares were initiated by hard γ -ray spikes whose $\sim 0.2 - 0.5$ s width is comparable to the Alfvén crossing time of the star, if the internal poloidal magnetic field is $\sim 10^{15}$ G (TD95). By contrast, a relaxation of the external magnetic field has a much shorter characteristic timescale $R_{\text{NS}}/c \sim 3 \times 10^{-5}$ s. This gives evidence that the giant flares are driven by the relaxation of *internal* magnetic stresses.

Any motion of the crust of a neutron star is strongly constrained by degeneracy and buoyancy forces, which resist bulk compressions and vertical displacements. A 10^{15} G magnetic field contributes only $\sim 10^{-4}$ of the hydrostatic pressure at the base of the crust. At the same time, it is capable of deforming the crust along equipotential surfaces of the star. Over large scales (kilometers or more), the lowest energy deformations of the crust involve a displacement field ξ which has a vanishing radial component and satisfies $\nabla \cdot (\rho \xi) = 0$, while maintaining a non-zero curl $\nabla \times (\rho \xi) \neq 0$.

Such a large-scale twisting motion of the crust, if it occurs suddenly, probably involves the formation of one or more propagating fractures. This type of deformation has been associated with the giant flares (Thompson et al. 2000; TD95). Since the magnetic potential

energy of twisting exceeds the crustal elastic energy (eq. [23]), the crust acts as a gate for the release of magnetic energy. The external magnetic field lines are anchored to the crust, so when the fracture occurs, the rapid turning motion does work on the external magnetic field. At the same time, it brings into contact regions of the crust where the magnetic field has differing strength and orientation, thereby creating strong field gradients and localized current sheets. Within the star, the bulk rotational motion also excites a helical Alfvén wave in the liquid core (where the magnetic field provides the dominant restoring force to a torsional motion). Torsional shear waves are excited in the rigid crust (McDermott et al. 1988; Duncan 1998), but are likely to carry less energy. We consider each of these physical elements in turn.

3.2.1. External Shear and Reconnection

Above the surface of the star, a disturbance of the magnetosphere propagates at very nearly the speed of light, which is some 300 times the shear wave speed V_μ in the deep crust. Thus, the external magnetic field can respond adiabatically to a *smooth* deformation of the crust. However, regions of the magnetosphere whose footpoints are strongly sheared can become subject to a purely magnetohydrodynamic instability (Lynden-Bell & Boily 1994; Mijic & Linker 1994). If localized near a fault, such an instability probably leads to reconnection and induces magnetohydrodynamic waves outside the star. Transverse Alfvén waves will have a characteristic frequency $\omega \sim c/x$ at a distance x from the fault. The corresponding wavenumbers are $k_\perp \gtrsim k_\parallel \sim x^{-1}$ in directions parallel and perpendicular to the background magnetic field. These waves can damp rapidly by cascading to a high wavenumber through non-linear interactions (Thompson & Blaes 1998). When the rate of transfer of wave energy (the ‘cascade luminosity’) exceeds a critical value ($\sim 10^4 L_{\text{edd}}$ within a volume of $\sim (10 \text{ km})^3$), the dissipated wave energy is locked onto the magnetic field lines in a thermal pair-photon plasma (TD95; Section 7 below). If excited directly in the magnetosphere, these waves are not easily reabsorbed by the crust, since crustal shear waves of the same frequency have a much larger wavenumber, by the ratio $c/V_\mu \sim 300$.

Thus, even though the giant flares are probably driven by internal magnetic stresses, the creation of a hot fireball outside the star involves the rapid relaxation of external magnetic stresses. This suggests that the energy released promptly in X-rays and γ -rays is roughly proportional to the *external* magnetic energy, after taking into account geometrical factors. Since a pure dipole field with polar strength $B_{15} \times 10^{15}$ G carries an energy $\sim 10^{47} B_{15}^2 (R_{\text{NS}}/10 \text{ km})^3$ ergs, the energy dissipated is small compared to the total external field energy if $B \sim 10^{15}$ G.

Suppose, for example, that a cap of the neutron star crust of radius ϖ were to rotate through an angle $\Delta\phi$, while the surrounding crust remains almost stationary. Even if this rotation were to be aligned with the axis of a purely dipolar field, one would expect strong shear to build up in the external field near the boundary of the cap. The amount of energy dissipated externally can be estimated, by supposing that this shear relaxes in N steps after a rotation through an angle $\Delta\phi/N$. The magnetic energy released in each step is then $\sim \pi\varpi^2(R_{\text{NS}}/3)(\delta B_{\text{NS}})^2/8\pi$, where $\delta B_{\text{NS}}/B_{\text{NS}} \sim \Delta\phi/N$ and we have assumed a dipole geometry with a radial scale length $R_{\text{NS}}/3$. The net energy which is available for powering X-rays and γ -rays is N times this,

$$\delta E_{\text{mag}} \sim \frac{(\Delta\phi)^2}{24N} \left(\frac{\varpi}{R_{\text{NS}}}\right)^2 B_{\text{NS}}^2 R_{\text{NS}}^3 = 4 \times 10^{45} \frac{(\Delta\phi)^2}{N} \left(\frac{\varpi}{3 \text{ km}}\right)^2 \left(\frac{B_{\text{NS}}}{10^{15} \text{ G}}\right)^2 \left(\frac{R_{\text{NS}}}{10 \text{ km}}\right) \text{ ergs.} \quad (26)$$

Thus the fraction of the star's surface area that experiences slippage in a giant flare could be as small as $(\pi\varpi^2)/(4\pi R_{\text{NS}}^2) \sim 0.02(\varpi/3 \text{ km})^2$ under favorable assumptions. If the position of the active region is determined by the large-scale winding of the internal magnetic field, then subsequent flares may occur at the same spot, and some of the surface may never flare. Alternatively, it is possible that independent regions encompassing no more than $N_{\text{flare}}^{-1} \sim 10^{-2}$ of the surface area flare only once over the active lifetime of an SGR. The peak luminosity of the initial spike is easily reproduced in this model, as long as δE_{mag} exceeds the observed value. This leads to a lower bound on the surface field, as discussed in (§5.2).

In a more realistic case, high-order multipoles of the field are present. This implies the existence of some exterior magnetic field lines which remain close to the star in a complex geometry. Stretching of field lines whose footpoints lie on opposite sides of a fault provides another mechanism for fast reconnection and flaring.

3.2.2. Internal Torsional and Standing Shear Waves

A twisting deformation of the neutron star crust, driven by the Maxwell stress $B_z B_\phi/4\pi$, will be accompanied by a partial unwinding of the core magnetic field. We consider, as before, a uniform poloidal flux density B_z threading the core. Then the core supports a torsional Alfvén mode, which propagates along the poloidal field with a period

$$P_{\text{Alfven}} \simeq \frac{4R_{\text{NS}}}{V_{Az}} = 0.4 \left(\frac{B_z}{10^{15} \text{ G}}\right)^{-1} \left(\frac{\rho}{10^{15} \text{ g cm}^{-3}}\right)^{1/2} \left(\frac{R_{\text{NS}}}{10 \text{ km}}\right) \text{ s} \quad (27)$$

near the symmetry axis. Here, $V_{Az} = B_z/\sqrt{4\pi\rho}$ is the poloidal Alfvén speed. This period receives a small correction from the shear strains that build up in the crust as the field that threads the crust/core boundary is twisted from below.

It should be noted that the mild density gradient in the neutron star core introduces a gradient in the wave period, with respect to the cylindrical radius ϖ . This gradient has the effect of washing out any quasi-periodicity in the wave motion – and thence in the dynamic stress applied to the crust – after a dozen or so wave periods.

Whether such a torsional Alfvén mode is strongly excited during a giant flare depends on the rate at which the crust deforms or breaks. Let us suppose that the core field untwists through an angle $\Delta\phi < \Delta\phi_0$, where the net twist across the core is

$$\Delta\phi_0(\varpi) = \frac{B_\phi(\varpi)}{B_z} \left(\frac{2R_{\text{NS}}}{\varpi} \right). \quad (28)$$

This formula can be expressed as

$$\Delta\phi_0(\varpi) = 0.3 \left(\frac{B_z}{10^{15} \text{ G}} \right)^{-2} \left(\frac{M_{\text{Coulomb}}}{0.02 M_\odot} \right) \left(\frac{V_{\mu 0}}{10^8 \text{ cm s}^{-1}} \right)^2 \left(\frac{\psi_{\text{cr}}}{10^{-2}} \right) \left(\frac{\varpi}{3 \text{ km}} \right)^{-2} \left(\frac{R_{\text{NS}}}{10 \text{ km}} \right)^{-1}, \quad (29)$$

in radians, making use of eq. (17). If the crust moves slowly, over a timescale Δt much larger than the Alfvén crossing time $2R_{\text{NS}}/V_{Az}$, then the amplitude of the resulting torsional wave is small. We estimate $\Delta\phi_{\text{wave}} \sim (\Delta\phi/\Delta t) \times (2R_{\text{NS}}/V_{Az})$, or equivalently

$$\frac{\Delta\phi_{\text{wave}}}{\Delta\phi} \sim \frac{2R_{\text{NS}}}{V_{Az}\Delta t}. \quad (30)$$

On the other hand, if the motion of the crust is slowed only slightly by friction (compared with a free torsional oscillation of the core) then a significant fraction of the released core magnetic energy goes into magnetic torsion modes. The fact that the observed durations of hard spikes in giant flares are comparable to a magnetar’s torsional oscillation period, $\sim 2R_{\text{NS}}/V_{Az} = \frac{1}{2}P_{\text{Alfvén}}$ for $\Delta\phi \sim \Delta\phi_0$, is consistent with the hypothesis that the crust *broke*, with only modest frictional resistance after the event onset. Significant torsional excitation of the neutron star core is thus plausible: $E_{\text{wave}} \sim E_X \sim 10^{44} - 10^{45}$ ergs.

A similar conclusion holds for the proportion of the crustal strain energy (11) which is converted to a torsional shear wave. The fundamental torsional mode (with $n = 0$ radial nodes) has an amplitude which varies weakly with depth in the crust (McDermott et al. 1988). Its harmonic is restricted to $\ell \geq 2$ from angular momentum conservation, and its period is

$$P_{n=0\ell} \simeq \frac{2\pi R_{\text{NS}}}{V_{\mu 0}[\ell(\ell+1)]^{1/2}} = 0.026 \left(\frac{R_{\text{NS}}}{10 \text{ km}} \right) \left(\frac{V_{\mu 0}}{10^8 \text{ cm s}^{-1}} \right)^{-1} \left[\frac{\ell(\ell+1)}{6} \right]^{-1/2} \text{ s}. \quad (31)$$

(This period is shifted downward slightly in the presence of a poloidal magnetic field, but the shift is not significant unless the component of the field along the direction of shear is comparable to $B_\mu \sim 6 \times 10^{15}$ G; Duncan 1998.) Notice that the period (31) is significantly shorter than the torsional Alfvén period (27). As a result, a significant fraction of the crustal strain energy would be converted *directly* to a torsional shear wave during a giant flare, only if this strain energy were released on a relatively short timescale compared with the duration of the hard spike, 0.03 s or less. Otherwise, the dynamic strain excited in the crust is dominated by the coupling to a torsional Alfvén mode in the core. In either case, the amplitudes of the shear wave and Alfvén wave can be expected to equilibrate rapidly (over a few wave periods) according to eq. (13), with the effect that the crustal shear wave has the lower energy by the factor (23).

3.2.3. External Torsional Deformation of the Magnetic Field

Such an internal torsional mode, with frequency $\omega = 2\pi/P_{\text{mode}}$ (eq. [27] or [31]), also drives a torsional excitation of the magnetic field outside the star. In the case of the crustal shear mode, we focus on the fundamental mode, whose amplitude varies weakly with depth below the surface of the neutron star (McDermott et al. 1988). The surface amplitude of the external magnetic twist is related to the surface displacement ξ of the crust through

$$\frac{\delta B_{\text{NS}}}{B_{\text{NS}}} = \frac{\omega \xi}{c}. \quad (32)$$

We now show that, in equilibrium, only a tiny fraction of the energy of the internal mode is transferred to the external mode. This energy transfer could take two forms: first, an Alfvén-like mode propagating freely on very extended field lines; and, second, a quasi-static torsional deformation of the field lines closer to the star, which oscillates in sign at the same frequency as the internal mode. Field lines which can support a propagating Alfvén mode have a minimum length cP_{mode} , and extend out to a large radius $R_{\text{max}} \gtrsim \frac{1}{3}cP_{\text{mode}}$ (in a dipole geometry). This works out to $R_{\text{max}} \sim 10^{10} (B_z/10^{15} \text{ G})^{-1}$ cm, using the period (27). These field lines are concentrated within a surface polar angle $\theta^2(R_{\text{NS}}) \lesssim 3R_{\text{NS}}/cP_{\text{mode}}$.

The internal mode will, in general, not be aligned with the external dipole moment, and so the surface shear will increase the external field energy by a fractional amount $\sim (\xi/R_{\text{NS}})^2$. This works out to $\delta E_{\text{mag}}(R > R_{\text{NS}}) \sim \frac{1}{12} B_{\text{NS}}^2 R_{\text{NS}}^3 (\xi/R_{\text{NS}})^2$ (here B_{NS} is the polar dipole field). Comparing with the elastic energy $E_{\text{elas}} = \frac{1}{2} \omega^2 \langle \xi^2 \rangle M_{\text{mode}}$ stored in the

crustal lattice, one finds

$$\frac{\delta E_{\text{mag}}(R > R_{\text{NS}})}{E_{\text{elas}}} = \frac{B_{\text{NS}}^2 R_{\text{NS}}^3}{6M_{\text{mode}}\omega^2 R_{\text{NS}}^2} = 5 \times 10^{-8} \left(\frac{B_{\text{NS}}}{10^{14} \text{ G}}\right)^2 \left(\frac{\omega R_{\text{NS}}}{c}\right)^{-2} \left(\frac{M_{\text{mode}}}{0.02 M_{\odot}}\right)^{-1} \left(\frac{R_{\text{NS}}}{10 \text{ km}}\right)^3. \quad (33)$$

This ratio is small in the case of a crustal shear mode ($M_{\text{mode}} \simeq M_{\text{Coulomb}} = 0.02 M_{\odot}$) and even smaller in the case of a torsional Alfvén mode ($M_{\text{mode}} \simeq M_{\text{NS}}$).

The equilibrium energy in the freely propagating Alfvén mode can easily be shown to be smaller than eq. (33) by a factor $\sim R_{\text{NS}}/R_{\text{max}} = 3R_{\text{NS}}/cP_{\text{mode}}$. Along the excited bundle of field lines, the product of the wave energy density $(\delta B)^2/8\pi$ and the cross-sectional area A of the field lines is a constant, and proportional to the square of the current $I(\theta)$ flowing at polar angles smaller than $\theta \sim (R_{\text{NS}}/R_{\text{max}})^{1/2}$. One has $I(\theta) = (c/4\pi)\pi\theta^2 R_{\text{NS}}^2(\nabla \times \mathbf{B})_R$, where the current density is related directly to the surface shear through $(\nabla \times \mathbf{B})_R \sim 2\pi(\xi/R_{\text{NS}})B_{\text{NS}}/R_{\text{NS}}$. The wave energy per length of field line is then proportional to θ^4 . Multiplying by the length $\sim 3R_{\text{max}}$ of the excited field lines gives a net energy proportional to $\theta^2 \sim R_{\text{NS}}/R_{\text{max}}$.

The damping rate of this external torsional mode is examined in §5.2, and compared with the observed peak luminosities of the giant flares.

3.2.4. Constraints from the Rise Time

The August 27th event showed a very steep rise in intensity, with width $t_{\text{rise}} \lesssim 4$ ms (Hurley et al. 1999a, Mazets et al. 1999). If this timescale is limited by the propagation of a fracture, then a triggering zone moving with fracture speed $V_f \lesssim V_{\mu}$ has size $l \gtrsim V_{\mu} t_{\text{rise}} = 4 \text{ km} (t_{\text{rise}}/4 \text{ ms})$. The fast rise of the 1979 March 5 event, $t_{\text{rise}} \lesssim 0.2$ ms (Cline et al. 1980; or $t_{\text{rise}} \sim 1$ ms as reported by Fenimore et al. 1996) may require that a fast magnetic reconnection front was generated in the magnetosphere at the onset of the event (Paczyński 1992). Alternatively, a fast rise could be understood if the large-scale, rotational motion results from self-organizing growth of collective motion in smaller-scale units in an “avalanche” effect. If these units have dimensions comparable to the depth of the crust, $\Delta R_{\mu} \sim 0.3$ km, then rise times as short as $\sim (\Delta R_{\mu}/V_{\mu}) \sim 3 \times 10^{-4}$ s are possible.

3.3. Giant Flares in the Context of SGR Activity

It has been argued that the giant flares involve a large-scale propagating fracture of the neutron star crust driven by magnetic stresses in the core (TD93; TD95). We have

described a specific configuration of the magnetic field, involving a strong twist in the core and crust, which can release $\sim 10^{44}$ ergs in individual increments as long as the yield strain in the gravitationally stratified crust is $\psi_{\text{cr}} \sim 10^{-2}$. Transport effects such as ambipolar diffusion acting on a timescale comparable to the source age of $\sim 10^4$ yr allow consecutive departures from magnetostatic equilibrium and repeated flaring activity, because unwinding of the core field is strongly inhibited by the compositional stratification of the neutron star interior. This is an efficient way to take magnetic free energy from its principal reservoir – a magnetic field anchored in the deep crust and core of a magnetar (see eq. [5]), and convert it to observable photon emissions, while evading the tremendous neutrino losses which are inevitable for all dissipation occurring locally in the interior.

The development of strong, localized shear in the exterior magnetic field allows the rapid dissipation of a large amount of magnetic energy *outside* the star, enough to power the observed flare emissions (eq. [26]). In addition, a significant fraction of the released energy may be deposited in a torsional Alfvén wave in the core, which transfers energy only gradually through the crustal lattice to the exterior. Moreover, a predominantly rotational deformation of the crust will leave behind non-potential terms in the exterior magnetic field which support persistent electrical currents which dissipate in part through Compton drag off the ambient X-ray flux (Thompson et al. 2000). The dramatic change in the non-thermal persistent flux and pulse shape of SGR 1900+14 following the August 27 giant flare (Woods et al. 2000) provides direct evidence for a strengthening of these non-potential components during the flare. More generally, such a corona has been hypothesized as the source of the persistent non-thermal emission in the SGRs and AXPs (TD96; Thompson et al. 2001), and for the transient non-thermal emission following the 29 August 1998 aftershock from SGR 1900+14 (§5.2.3 in Ibrahim et al. 2000).

Shorter $\sim 1 - 10$ s bursts were observed soon after the two giant flares (see Mazets et al. 1979a for SGR 0525-66, and Ibrahim et al. 2000 for SGR 1900+14), with luminosities comparable to the pulsating tails of the flares. In the above model, these shorter bursts probably involve shorter fault-line slippage than the flares. The relation of the much more common ~ 0.1 s SGR bursts to the giant flares is perhaps more mysterious; while these events could also involve a propagating fracture, they may alternatively be driven by a more localized and plastic deformation of the crust (TD95).

4. Soft Pulsations: the Light Curve

The hard spike and the extended soft tail of the August 27 event released comparable energies, $E \sim (0.5 - 1) \times 10^{44}$ ergs, even though their durations differed by a factor of 10^3 .

This suggests that a large fraction of the outburst energy was injected during the initial ~ 0.5 s. Whereas the enormous luminosity of the spike requires a relativistic outflow from the neutron star, the spectral stability and large amplitude oscillations observed during the last ~ 300 s of the outburst require instead that the radiated energy was confined close to the surface of the neutron star. This energy, if released into the near magnetosphere, forms a dense, thermal plasma of e^\pm pairs and blackbody radiation with a temperature $T = 0.72 (E/10^{44} \text{ ergs})^{1/4} (L/10 \text{ km})^{-3/4} \text{ MeV}$ (in a volume L^3). The scattering opacity of electrons and positrons was then high enough to lock this energy onto magnetic field lines close to the neutron star, in a “trapped fireball”. This fireball cools by radiative diffusion through a thin surface layer, which contracts inward while remaining nearly congruent with the magnetic field (TD95).

Strong evidence for this trapped fireball model comes from the faster-than-exponential decline in the X-ray flux at the end of the August 27 outburst, which is consistent with the hypothesis that the energy reservoir is evaporating completely in a finite time. Except for the first ~ 40 s (one tenth of the burst duration), the envelope of the August 27 light curve is well fit by the following function (Paper I)

$$L_X(t) = L_X(0) \left(1 - \frac{t}{t_{\text{evap}}}\right)^\chi. \quad (34)$$

If the cooling luminosity is assumed to vary as a power of the *remaining* fireball energy, $L_X \propto E^a$, then $\chi = a/(1 - a)$. In the simplest case of a fireball with uniform energy density and surface energy flux, the index χ is effectively the number D_c of curved directions of the fireball surface: $\chi = D_c = 2$ for a spherical fireball; $\chi = D_c = 1$ for a fireball filling bundle of flux lines that is (locally) cylindrical; and $\chi = D_c = 0$ for the case of a bundle of flux lines that is (locally) a thin slab (Fig. 3).

This function (34) accurately captures the sudden final drop in flux seen in the *Ulysses* and BeppoSAX data (Paper I). The best-fit fireball index is $\chi = 3$ (or $a = 0.75$), and the evaporation time $t_{\text{evap}} = 375$ s (Figs. 2-3 of Paper I). Note that the fit is excellent following the initial ~ 40 -s of the outburst. In comparison, the best fit exponential profile $\exp(-t/t_{\text{exp}})$ adequately describes the intermediate portion of the decay (Fig. 1. of Paper I), with a favored time constant $t_{\text{exp}} = 78$ s in the *Ulysses* data; but significantly overshoots the final ~ 40 s of the outburst.

During the first ~ 40 s, the measured burst flux significantly overshoots both the exponential and trapped fireball fitting functions. The mild spin-modulation of the light curve during this smooth tail requires a more extended and variable photosphere. which we argued in Paper I is pair-dominated and results from a continuing creep of the neutron star crust in the active region (or possibly a standing torsional wave in its interior). The cooling

of a continuously heated, pair-dominated corona is discussed in detail in §7.

4.1. Fireball Index

We now consider some simple physical models for a contracting fireball. Because the best-fit fireball index χ is larger than 2 (the maximum number of curved directions for the fireball surface in three spatial dimensions), a homogeneous fireball cannot explain the data. In this section, we consider the effects of temperature and magnetic field gradients.

The surface of the fireball will be assumed to have D_c curved directions and $2 - D_c$ flat directions, and to be fully symmetric with a single perpendicular coordinate r . Before the cooling wave propagates into the fireball, the temperature and magnetic field vary as powers of r :

$$T \propto r^\gamma ; \quad B \propto r^\beta. \quad (35)$$

Temperature gradients perpendicular to \mathbf{B} easily persist over the duration of the August 27 event, because the photon diffusion time across a distance $\sim R_{\text{NS}}$ through the fireball is much larger than the observed burst duration (or the time for the cool boundary layer to propagate into the fireball: TD95 §3.2 and §3.4).

If the surface flux from a trapped fireball varies as

$$F \propto T^{\sigma_1} B^{\sigma_2}. \quad (36)$$

then, because the emitting area scales as $A \propto r^{D_c}$, the luminosity is

$$L_X = L_X(0) \left(\frac{r}{r_0} \right)^{D_c + \sigma_1 \gamma + \sigma_2 \beta}. \quad (37)$$

The energy density within the fireball includes contributions from both photons and electron-positron pairs. In two regimes of relevance, it has the form

$$U \propto T^{\mu_1} B^{\mu_2}. \quad (38)$$

In particular, if many Landau levels are populated and $T \gg m_e$, then one recovers the usual expression for a relativistic pair plasma, $U = (11/4)aT^4$ where a is the Stefan-Boltzmann constant, and $\mu_1 = 4$ and $\mu_2 = 0$. The condition for a such 3-dimensional pair gas is⁶ $2.7T \gtrsim (2eB)^{1/2}$ or equivalently

$$T \gtrsim 0.3 \left(\frac{B}{B_{\text{QED}}} \right)^{1/2} \text{ MeV} \quad (39)$$

⁶In units with $\hbar = 1 = c$, used frequently hereafter.

in a magnetic field $B \gtrsim B_{\text{QED}}$ (eq. 1). This condition is easily satisfied near marginal confinement, when the pressure of pairs and photons is close to the limiting value $B^2/8\pi$ (TD95).

When the magnetic pressure greatly exceeds the thermal pressure, and T is not much less than m_e , the pairs dominate the thermal energy density: $U \approx U_{e^+e^-} \approx (1/12)eBT^2$ (in units where $\hbar = c = 1$). The indices μ_i are then $\mu_1 = 2$ and $\mu_2 = 1$ [see eq. (53) and the discussion following eq. (56) in TD95; see also Figure 5 in Duncan 2000 and Kudari 1997].

The surface X-ray luminosity is related to surface area A of the fireball and its rate of contraction through $L_X = -AU(dr/dt)$, or

$$L_X = -L_X(0) \left(\frac{r}{r_0} \right)^{D_c + \mu_1 \gamma + \mu_2 \beta} \frac{dr/dt}{(dr/dt)_0}. \quad (40)$$

Equations (37) and (40) together give a simple differential equation for $r(t)$. The solution implies that $L_X(t)$ has the form of eq. (34) with

$$\chi = \frac{D_c + \sigma_1 \gamma + \sigma_2 \beta}{1 + \gamma(\mu_1 - \sigma_1) + \beta(\mu_2 - \sigma_2)} \quad (41)$$

The case of a structureless trapped fireball, $\gamma = \beta = 0$, reduces to $\chi = D_c \leq 2$. Since $\chi \simeq 3$ empirically, we infer that the fireball must have had structure, with indices which satisfy

$$(3\mu_1 - 4\sigma_1)\gamma + (3\mu_2 - 4\sigma_2)\beta = D_c - 3. \quad (42)$$

Specific values of the structure indices γ and β , for several plausible assumptions about the fireball geometry and physical conditions, are given in Table 1.

These values of γ and β depend on specific choices for the parameters σ_i in the surface X-ray flux (36) from the trapped fireball. One generally expects a positive dependence on temperature and magnetic field because of the thermal nature of the emission ($\sigma_1 > 0$), and because Compton scattering is suppressed in a strong magnetic field ($\sigma_2 > 0$). We have considered three cases which span the possible range of cooling-wave behaviors: one case in which F is most sensitive to B ; one in which F is sensitive to T , and one with sensitivity to both variables. The case $\sigma_1 = 0$, $\sigma_2 = 4/3$ corresponds to a simple Eddington-limited flux from an atmosphere that is held down by gravity, when the magnetic suppression of scattering is taken into account (eqs. [45] and [93] in TD95). The case $\sigma_1 = 5/2$, $\sigma_2 = 0$ corresponds to a magnetically-confined fireball in which the confined plasma fills many Landau levels ($\mu_1 = 4$, $\mu_2 = 0$), and in which the integrated surface flux across \mathbf{B} is limited by the rate at which energy is advected *along* the magnetic field, so as to smooth out

pressure imbalances (eq. [89] of TD95). Finally, the case $\sigma_1 = 3/2$, $\sigma_2 = 1$ (eq. [86] of TD95) corresponds to a similar process of advection-limited cooling, but in the opposite regime where the confined plasma is too cool to fill higher Landau levels (so that the radiative opacity across \mathbf{B} is suppressed by the strong magnetic field). In these last two cases, T is interpreted as the temperature just inside the geometrically-thin radiative layer at the surface of the fireball.

Table 1 shows that, in all physical regimes considered, a fireball that is slightly hotter in the center than near the edges, $\gamma < 0$, can fit the observed light curve. Such a pattern of energy-loading in the magnetosphere could plausibly occur. An alternative, less attractive possibility, is that the temperature inside the fireball is uniform while the magnetic field *declines* slightly toward its center, $\beta > 0$.

4.2. Effects of Neutrino Cooling

The trapped fireball light curve will also be perturbed by neutrino pair emission, $e^+ + e^- \rightarrow \nu + \bar{\nu}$, at a rate $\dot{U}(e^+e^- \rightarrow \nu\bar{\nu}) = 1.3 \times 10^{25} (T/\text{MeV})^9 \text{ ergs cm}^{-3} \text{ s}^{-1}$ (Dicus 1972; Schinder et al. 1987). This can reduce the fireball energy on a time scale comparable to the duration of the giant outburst (§5 in TD95):

$$\tau_\nu \equiv \frac{\frac{11}{4}aT^4}{\dot{U}(e^+e^- \rightarrow \nu\bar{\nu})} = 28 \left(\frac{T}{1 \text{ MeV}} \right)^{-5} \text{ s.} \quad (43)$$

This expression assumes that the temperature is high enough to excite pairs in the upper Landau levels (eq. [39]).

The effects of pair neutrino cooling on a fireball light curve are shown in Figs. 4a and 4b for several initial values of the dimensionless ratio $(E/L_X\tau_\nu)$ and a fixed evaporation time t_{evap} . In Fig. 4a, we plot fireball light curves for various geometries ($D_c = 1, 2$), assuming that the trapped pair gas is 3-dimensional ($\mu_1 = 4$, $\mu_2 = 0$) and that the cooling wave is limited by advection ($\sigma_1 = 5/2$, $\sigma_2 = 0$; see eq. [89] in TD95). The neutrino cooling time is parameterized by the initial value of the dimensionless ratio $E/L_X\tau_\nu$, where E is the trapped fireball energy. One sees that neutrino cooling introduces additional curvature in the (logarithmic) light curve, predominantly during the initial decline. This curvature is absent for a homogeneous fireball ($\gamma = \beta = 0$), as well as for a fireball with powerlaw temperature and magnetic field profiles (constant γ , β). In Fig. 4b, we consider a combination of neutrino cooling and temperature gradients, with the value of γ perturbed slightly from the best-fit value (42). (Here the initial value of $(E/L_X\tau_\nu)$ is calculated using the initial temperature at the outer boundary of the fireball.)

To summarize: neutrino cooling introduces curvature in the trapped-fireball light curve, which cannot be compensated by a power-law temperature gradient. A large value of $(E/L_X\tau_\nu) \gtrsim 10$ does not fit the observed light curve, but one can not rule out a combination of slower neutrino cooling and more complicated temperature profiles.

5. Bound on the Stellar Dipole Moment

In this section, we quantify how the long duration and enormous peak luminosity of a giant flare set lower bounds to the magnetic moment of its source. First, by including the effects of neutrino cooling on the declining X-ray flux of a trapped pair-photon plasma, we are able to set a lower bound on B_{dipole} that is less dependent on assumptions about the configuration of the field than those made in TD95. Second, by considering in more detail the coupling between a low-frequency internal (e.g. torsional) mode of the star and its magnetosphere, we are able to show that such a low-frequency mode cannot easily lose energy at the rate observed in the hard initial spike: even under the most optimistic assumptions about the damping of the external magnetic shear, the surface flux density must be very high (in excess of 10^{14} G).

5.1. Confinement of the Radiating Plasma During the Soft Pulsations

A strong lower bound on the surface magnetic field is deduced from confinement of a large amount of energy, $E \sim 10^{44}$ ergs, close to the SGR source during a giant flare. Assuming that the field is a centered dipole, and requiring that $B^2/8\pi > P_\gamma + P_{e\pm}$ at the outer boundary of the fireball, one deduces

$$B_{dipole} > 2 \times 10^{14} \left(\frac{E_{\text{fireball}}}{10^{44} \text{ ergs}} \right)^{1/2} \left(\frac{\Delta R}{10 \text{ km}} \right)^{-3/2} \left[\frac{1 + \Delta R/R_{\text{NS}}}{2} \right]^3 \text{ G} \quad (44)$$

for a relativistic plasma (TD95). Here ΔR is the characteristic size of the fireball.

The question which next arises, is how this bound is modified if the magnetic field is not a centered dipole. Indeed, the remarkable four-peaked pattern of the August 27 pulsating tail provides direct evidence for higher multipoles (Paper I; Section 8). Consider first how this bound is modified as the footpoints of the confining magnetic field are brought closer together. The minimum pressure of the confining magnetic field increases with decreasing footpoint separation L , $B_{\text{min}}^2/8\pi \sim E/3L^3$, but the net magnetic moment of the confining field *decreases*, $\mu_{\text{min}} \sim B_{\text{min}}L^3 \propto E^{1/2}L^{3/2}$. At the same time, the temperature of the confined plasma (assumed to have a 3-D distribution) increases, $T \propto L^{-3/4}$.

The bound on B_{dipole} cannot, however, be reduced arbitrarily by shrinking the fireball. The reason is that the neutrino cooling time of the fireball decreases rapidly with decreasing L ,

$$\tau_\nu \propto T^{-5} \propto L^{15/4} \quad (45)$$

at fixed energy E , even while the photon cooling time (eq. [34]) hardly changes:

$$t_{\text{evap}} \sim L/V_{\text{cool}} \sim L^{-1/8} \quad (46)$$

in the absence of neutrino cooling. (The propagation speed of the cool boundary is related to the surface X-ray flux by $V_{\text{cool}} = F_X(T)/[\frac{11}{4}aT^4] \propto T^{-3/2}$.)

To get a sense of how far B_{dipole} can be reduced and remain consistent with magnetic confinement of the radiating plasma, let us consider a small offset dipole, centered at the outer edge of the star (Fig. 3). Neutrino cooling has a large effect on the fireball lightcurve when $\tau_\nu \lesssim t_{\text{evap}}$, where the evaporation time can be written as

$$t_{\text{evap}} = (\chi + 1) \left(\frac{E}{L_X} \right)_0. \quad (47)$$

Indeed, in the case of rapid neutrino cooling, one can divide the cooling process into two phases: an initial neutrino-dominated phase where the fireball volume hardly decreases; and a subsequent photon-dominated cooling phase. Integrating the neutrino losses up to a time $\sim t_{\text{evap}}/(\chi + 1)$, the fireball pressure is reduced by a factor

$$\frac{P_{e^\pm} + P_\gamma}{(P_{e^\pm} + P_\gamma)_0} = \left(\frac{T}{T_0} \right)^4 = \left[1 + \frac{5}{4} \left(\frac{E}{L_X \tau_\nu} \right)_0 \right]^{-4/5} \quad (48)$$

Thus, as $E/L_X \tau_\nu \propto L^{-31/8}$ is pushed above unity, the lower bound on the magnetic moment does not change significantly: $\mu_{\text{min}} \propto (E_0 L^3)^{1/2}$ is almost independent of L . For the purposes of estimating μ_{min} , we conservatively take $(E/L_X \tau_\nu)_0 = 10$ in what follows. This corresponds to $\tau_\nu \gtrsim 0.025 t_{\text{evap}}$ when $\chi = 3$.

This lower bound on the neutrino cooling time yields an *upper* bound on the fireball temperature through eq. (43),

$$T_{\text{max}} = 1.2 \left(\frac{t_{\text{evap}}}{400 \text{ s}} \right)^{-1/5} \text{ MeV}. \quad (49)$$

In order to contain the energy radiated in the August 27 pulsating tail, the volume of the fireball must exceed

$$V_{\text{fireball}} = \frac{E}{(11/4)aT^4} = (4.9 \text{ km})^3 \left(\frac{E}{10^{44} \text{ ergs}} \right) \left(\frac{T}{T_{\text{max}}} \right)^{-4} \left(\frac{t_{\text{evap}}}{400 \text{ s}} \right)^{4/5}. \quad (50)$$

The confining magnetic field at its weakest point must be stronger than $B_{\min}^2/8\pi = P_\gamma + P_{e\pm} = \frac{11}{12}aT^4$, which combined with eq. (49) implies $B_{\min} = 8.3 \times 10^{13}(T/T_{\max})^2(t_{\text{evap}}/400 \text{ s})^{-2/5}$ G. Given that the plasma fills half the dipole magnetic field, and only along field lines which never drop below this flux density, the magnetic moment can be calculated to be

$$\mu_{\min} = \frac{105}{32\pi} B_{\min} V_{\text{fireball}} = 1 \times 10^{31} \left(\frac{E}{10^{44} \text{ ergs}} \right) \left(\frac{T}{T_{\max}} \right)^{-2} \left(\frac{t_{\text{evap}}}{400 \text{ s}} \right)^{2/5} \text{ G} - \text{cm}^3. \quad (51)$$

In this expression, B_{\min} is the minimum flux density at the magnetic equator.

This expression provides only a lower bound to the *net* dipole moment of the neutron star, for two reasons. First, no change was observed in the spindown rate of SGR 1900+14 in the few months following the August 27 event (Woods et al. 1999), which implies that the dipole moment of the confining magnetic field was only a fraction of the total (Thompson et al. 2000). A conservative upper bound of ~ 30 percent to the fractional change in \dot{P} translates into a maximum change $\delta\mu_{\text{net}}/\mu_{\text{net}} \sim 0.15$ in the magnetic moment in the case of magnetic dipole spindown ($\dot{P} \propto \mu_{\text{net}}^2$). The tolerable change in the magnetic moment could be larger, $\delta\mu_{\text{net}}/\mu_{\text{net}} \sim 0.3$, if the spindown were accelerated by a persistent wind of particles and Alfvén waves, assuming that the wind’s power L_W does not change across the flare ($\dot{P} \propto \mu_{\text{net}} L_W^{1/2}$; Thompson & Blaes 1998; Harding et al. 1999; Thompson et al. 2000). On the other hand, the giant outburst is expected to produce a change $\delta\mu_{\text{net}}/\mu_{\text{net}} \sim \mu_{\min}/\mu_{\text{net}}$ in the net magnetic moment, and so we arrive at

$$\mu_{\text{net}} \gtrsim \left(\frac{\delta\mu_{\text{net}}}{\mu_{\text{net}}} \right)^{-1} \mu_{\min} = 2 \times 10^{32} \left(\frac{\delta\mu_{\text{net}}/\mu_{\text{net}}}{0.1} \right)^{-1} \left(\frac{E}{10^{44} \text{ ergs}} \right) \left(\frac{T}{T_{\max}} \right)^{-2} \text{ G} - \text{cm}^3. \quad (52)$$

In this case, the effective polar dipole field is

$$B_{\text{dipole}} = \frac{2\mu_{\text{net}}}{R_{\text{NS}}^3} \gtrsim 4 \times 10^{14} \left(\frac{E}{10^{44} \text{ ergs}} \right)^{1/2} \left(\frac{T}{T_{\max}} \right)^{-2} \left(\frac{R_{\text{NS}}}{10 \text{ km}} \right)^{-3} \text{ G}. \quad (53)$$

A single dipole of magnitude (52) barely contains enough energy to power a single giant outburst, which suggests that either the entire external field of SGR 1900+14 was strongly sheared during the flare; or the actual field is much stronger than (53); or the surface of the star is covered with many dipoles $\gtrsim \mu_{\min}$. If the net energy output in N giant flares is comparable to the external magnetic energy, then we estimate

$$\mu_{\text{net}} \gtrsim N^{1/2} \mu_{\min} = 1 \times 10^{32} \left(\frac{N}{100} \right)^{1/2} \left(\frac{E}{10^{44} \text{ ergs}} \right) \left(\frac{T}{T_{\max}} \right)^{-2} \left(\frac{t_{\text{evap}}}{400 \text{ s}} \right)^{2/5} \text{ G} - \text{cm}^3. \quad (54)$$

(Note that this expression describes both a single large dipole, and also the incoherent superposition of N mini-dipoles of magnitude μ_{\min} ; see also §12.3 in TD93.)

5.2. Peak Luminosity and Bound on the Surface Magnetic Field

The initial spike of the August 27 flare reached a peak luminosity⁷ $L \gtrsim 10^{44}$ ergs s⁻¹ (Mazets et al. 1999), approaching a million times the Eddington luminosity of a neutron star. Such a high rate of release of energy allows us to set a stringent lower bound on the magnetic field in the source, which is compatible with the value deduced from the total expected flaring output (§2). Note that the opacity of the emitting material is not directly relevant to this bound, since the hard spike appears to have involved an expanding fireball.

Motions of a neutron star crust will release magnetic energy directly by inducing tangential discontinuities in the field, which lead to fast reconnection and high frequency wave motion (Thompson 2000; §3.2.1 above). The output induced by a horizontal motion through a distance $\sim R_{\text{NS}}$ over a timescale Δt_{spike} is $L_{\text{spike}} \sim \epsilon_X (B^2/8\pi) R_{\text{NS}}^3 / \Delta t_{\text{spike}}$. Here ϵ_X is the fraction of the magnetic energy which is dissipated and converted to high energy photons, and is estimated in eq. (26). The implied r.m.s magnetic field is

$$B \gtrsim 2 \times 10^{14} \left(\frac{\epsilon_X}{0.1} \right)^{-1/2} \left(\frac{\Delta t_{\text{spike}} L_{\text{spike}}}{10^{44} \text{ ergs}} \right)^{1/2} \text{ G.} \quad (55)$$

Much of the dissipated energy would initially be confined by the (dipole) magnetic field. Nonetheless, the confined pair plasma generated in such a giant flare can easily exceed the dipole pressure (which decreases as R^{-6}) at a short distance above the surface of the neutron star. This provides a mechanism for driving a relativistic, pair-loaded fireball. The rise time of the August 27 hard spike could, in fact, be limited by the breakout of this confined pair plasma. Evidence for repeated breakouts of pair plasma is provided by the ~ 20 ms modulation of the hard spike of the March 5 event (Barat et al. 1983).

Let us also examine the alternative possibility that the magnetic field merely acts as a couple between an internal mode of the neutron star and external Alfvén-like excitations. Of the possible internal modes of a neutron star, a crustal shear wave has the strongest coupling to the magnetosphere (Blaes et al. 1989). The required magnetic field turns out to be similar, even after making the most optimistic assumptions about the damping rate of the external mode. This is because the field lines are anchored in very dense material, within which a shear disturbance propagates much more slowly than it does in the magnetosphere. (Equivalently, the equilibrium energy stored in the external mode is a tiny fraction of the energy in the internal mode; §3.2.2.) A related mechanism involving the

⁷This applies after allowing for dead-time corrections; this value remains below that inferred previously for the peak luminosity of the March 5 event at the distance of the LMC (Mazets et al. 1979).

coupling of an internal p - or f -mode to the magnetosphere was examined soon after the 5 March 1979 flare, by Ramaty et al. (1980) and Lindblom & Detweiler (1983). As we argue below, the damping rate was significantly overestimated by these authors, and is in fact much closer to the rate for vacuum dipole radiation.

Global toroidal modes in the crust can be excited directly through a large-scale fracture, as is expected in a giant flare, or indirectly through coupling to a torsional Alfvén mode in the core (§3.2.2; Duncan 1998). The fundamental toroidal mode (with $n = 0$ radial nodes) has a frequency $\omega \simeq \sqrt{\ell(\ell + 1)}(V_{\mu 0}/R_{\text{NS}})$ for $\ell \geq 2$ (McDermott et al. 1988). Whereas the torsional Alfvén mode has a frequency $\omega = \pi V_{A,z}/2R_{\text{NS}}$ (in a uniform poloidal magnetic field B_z with corresponding Alfvén speed $V_{A,z} = B_z/\sqrt{4\pi\rho}$; eq. [27]). To begin, let us consider an excitation confined to the crust. Suppose that an energy $E_{\text{elas}} \sim 10^{44}$ ergs was deposited in toroidal modes (of various harmonics ℓ) during the initial ~ 0.5 s spike. The r.m.s. mode amplitude $\langle \xi^2 \rangle^{1/2}$ at the neutron star surface is related to the mode energy E_{elas} by substituting $\psi^2 \simeq \ell(\ell + 1)(\xi/R_{\text{NS}})^2$ in equation (6), which gives $E_{\text{elas}} = \frac{1}{2}\ell(\ell + 1) M_{\text{Coulomb}} V_{\mu 0}^2 (\xi/R_{\text{NS}})^2$. We have in turn

$$\langle \xi^2 \rangle^{1/2} = 0.1 \left(\frac{E_{\text{elas}}}{10^{44} \text{ ergs}} \right)^{1/2} \left[\frac{\ell(\ell + 1)}{6} \right]^{-1/2} \left(\frac{M_{\text{Coulomb}}}{0.02 M_{\odot}} \right)^{-1/2} \left(\frac{V_{\mu 0}}{10^8 \text{ cm s}^{-1}} \right) \text{ km.} \quad (56)$$

The resulting harmonic displacement of the neutron star magnetosphere can be divided into two components (§3.2.3): a quasi-static deformation of field lines which close within a radius $R_{\text{max}} \sim \frac{1}{3}c(2\pi/\omega)$; and an Alfvén mode which propagates freely along more extended field lines, with a group velocity $d\omega/d\mathbf{k} = c\hat{B}$.

To set a conservative *lower* bound on the rate of dissipation of energy in the magnetosphere, let us assume that the quasi-static twist is damped within a substantial solid angle $\Delta\Omega$ on a short timescale $2\pi/\omega \gtrsim t_{\text{damp}} \gtrsim R_{\text{NS}}/c$. (Notice that the light-crossing time R_{NS}/c is much shorter than the mode period, by a factor $\sim V_{\mu 0}/c$.) The amplitude of the deformed field grows at a rate $d\delta B_{\text{NS}}/dt \sim (\omega\xi/R_{\text{NS}})B_{\text{NS}}$, leading to an equilibrium amplitude $\delta B_{\text{NS}}/B_{\text{NS}} \sim (ct_{\text{damp}}/R_{\text{NS}})(\omega\xi/c)$. The torsional mode energy then decreases at the rate

$$-\frac{dE_{\text{elas}}}{dt} \simeq (\Delta\Omega R_{\text{NS}}^2) \frac{B_{\text{NS}}^2}{8\pi} c \left(\frac{\omega\xi}{c} \right)^2 \left(\frac{ct_{\text{damp}}}{R_{\text{NS}}} \right). \quad (57)$$

This expression is maximized at a damping time $t_{\text{damp}} \sim P_{\text{mode}} = 2\pi/\omega$ (above which the damping rate scales inversely with t_{damp}). It can be inverted to yield the *minimum* mode energy needed to power a given rate of dissipation, which we set equal to the spike

luminosity L_{spike} :

$$E_{\text{elas}} = 1 \times 10^{43} \left(\frac{L_{\text{spike}}}{10^{44} \text{ ergs s}^{-1}} \right) \left(\frac{P_{\text{mode}}}{0.03 \text{ s}} \right)^{-1} \left(\frac{B_{\text{NS}}}{10^{14} \text{ G}} \right)^{-2} \left(\frac{M_{\text{Coulomb}}}{0.015 M_{\odot}} \right) \left(\frac{\Delta\Omega}{4\pi} \right)^{-1} \text{ ergs s}^{-1}. \quad (58)$$

One sees that even if the mode is damped over a large solid angle $\Delta\Omega \sim 4\pi$, a surface magnetic field of at least $B_{\text{NS}} \sim 3 \times 10^{13} (P_{\text{mode}}/0.03 \text{ s})^{-1/2} \text{ G}$ is required. Otherwise, the mode must carry much more energy than is radiated. Indeed, crustal shear oscillations are barely capable of storing sufficient energy (eq. [11]).

It is perhaps more natural for a large energy to be deposited in a torsional Alfvén mode in the liquid interior, for the reasons discussed in §3.2.2. The mode energy would then be even larger, $E_{\text{Alfvén}} \sim \frac{1}{2} M_{\text{NS}} (\xi \omega_{\text{Alfvén}})^2$. In order to power the hard spike via Alfvén waves from the excited star, a condition similar to eq. (58) must be satisfied, but with the mode mass M_{Coulomb} replaced by M_{NS} . The lower bound on the magnetic field is then more severe, $B_{\text{NS}} \gtrsim 3 \times 10^{14} (P_{\text{mode}}/0.03 \text{ s})^{-1/2} \text{ G}$.

These bounds on the mode energy are conservative: it is less than clear that a smooth periodic deformation of the external magnetic field will damp in a time as short as P_{mode} , and only a small fraction $\sim 3R_{\text{NS}}/cP_{\text{mode}}$ of the external field lines are able to support a propagating shear Alfvén mode with a frequency comparable to that of the internal mode. By contrast, dissipation will occur effectively outside the star through the build-up of strong, localized shear (e.g. near the site of a fracture).

Could an internal toroidal mode power the more modest output of $L_X \sim 10^{42} \text{ ergs s}^{-1}$, above and beyond the trapped-fireball light curve, which is observed during the initial $\sim 40 \text{ s}$ of the August 27 flare? We ascribed this excess emission to a continuously heated pair-dominated corona in Paper I. (Fatuzzo & Melia (1993) and Melia & Fatuzzo (1995) have explored the related possibility that short SGR bursts may be powered by the continuous dissipation of sheared Alfvén waves propagating away from a more weakly magnetized neutron star, but did not address the relation between the Alfvén wave flux and the mode energy.) Setting the mode energy equal to this excess X-ray output of $\sim 10^{43} \text{ ergs}$, one deduces from equation (58) that the external Alfvén mode must be damped through a solid angle $\Delta\Omega \simeq 4\pi (B_{\text{NS}}/10^{14} \text{ G})^{-2} (P_{\text{mode}}/0.03 \text{ s})^{-1} (M_{\text{mode}}/M_{\text{NS}}) \text{ Sr}$. For the reasons just described, this angle is uncomfortably but not impossibly large. The excess emission during the first $\sim 40 \text{ s}$ could, alternatively, have been powered by a continued shearing of the external magnetic field, driven by a diminishing creep of the crust in the active region; or by the gradual decay of static magnetospheric currents.

Finally, let us compare our results with the model of Ramaty et al. (1980) and Lindblom & Detweiler (1983). It was suggested in these papers that an internal f - or

p -mode would be damped by shock-heating of the surface layers of the neutron star, and also by a strong flux of Alfvén waves into the magnetosphere. Repeated shocking of the surface layers of a star can occur only if the time for a sound wave to cross a pressure scale-height is *longer* at shallower depths. (Otherwise, an upward-propagating sound wave will be reflected downward before it has a chance to steepen into a shock.) This condition is indeed satisfied in the envelope of a pulsating AGB star, but it fails to be satisfied in the crust of a neutron star. We start with the equation of hydrostatic equilibrium, $dP/dr = -\rho GM(< r)/r^2$, where $P(z) \propto [\rho(z)]^\gamma$ at depth $z = R_{\text{NS}} - r$. (The index $\gamma \simeq \frac{4}{3}$ for $\rho \sim 10^6 - 4 \times 10^{11}$ g cm $^{-3}$ and $\gamma \simeq \frac{5}{3}$ at lower densities.) Integrating gives $P(z)/\rho(z) \simeq (\gamma - 1) z (GM_{\text{NS}}/R_{\text{NS}}^2)$, along with the sound speed $c_s \simeq \sqrt{\gamma P/\rho}$ and the pressure scale-height $\ell_P = P/(-dP/dr)$ as functions of depth. In a neutron star, the sound-crossing time decreases outward,

$$\frac{\ell_P}{c_s} = \left(\frac{\gamma - 1}{\gamma} \right)^{1/2} \left(\frac{z}{R_{\text{NS}}} \right)^{1/2} \left(\frac{R_{\text{NS}}^3}{GM_{\text{NS}}} \right)^{1/2}, \quad (59)$$

and so the surface layers are manifestly stable to repeated shocking.

Now let us consider the electromagnetic damping of an f - or p -mode. The damping rate into Alfvén waves is even lower, because an f - or p -mode does not shear the external magnetic field lines. The mode could have a frequency as high as $\omega \sim 10^4$ Hz, and so a much wider bundle of external field lines would be excited than by a lower-frequency torsional mode. (We assume for now that the magnetosphere is able to respond to the surface motions as a conducting fluid.) To set a conservative upper bound on the energy flux into the magnetosphere, we allow all the field lines to carry away Alfvén waves of an amplitude $\delta B_{\text{NS}}/B_{\text{NS}} = \xi\omega/c$ and a surface energy flux $c(\delta B_{\text{NS}})^2/8\pi$. The mode energy $E_{\text{mode}} \simeq \frac{1}{2}M_{\text{NS}}\omega^2\langle\xi^2\rangle$ is then damped at a rate

$$-\frac{dE_{\text{mode}}}{dt} \simeq 4\pi R_{\text{NS}}^2 c \frac{B_{\text{NS}}^2}{8\pi} \left(\frac{\omega^2\langle\xi^2\rangle}{c^2} \right) = \frac{E_{\text{mode}} R_{\text{NS}}^2 B_{\text{NS}}^2}{M_{\text{NS}} c}. \quad (60)$$

For a neutron star mass $M_{\text{NS}} = 1.4 M_\odot$ and radius $R_{\text{NS}} = 10$ km, this expression becomes

$$-\frac{dE_{\text{mode}}}{dt} \simeq 1 \times 10^{42} \left(\frac{E_{\text{mode}}}{10^{44} \text{ ergs}} \right) \left(\frac{B_{\text{NS}}}{10^{15} \text{ G}} \right)^2 \text{ ergs s}^{-1}. \quad (61)$$

As a check, consider the damping rate due to vacuum dipole radiation. As before, we normalize the mode energy $E_{\text{mode}} \simeq \frac{1}{2}M_{\text{NS}}\xi^2\omega^2$ to the observed X-ray output of the flare. One has

$$-\left(\frac{dE_{\text{mode}}}{dt} \right)_{\text{MDR}} = \frac{2\omega^4}{3c^3} \mathcal{M}^2 \left(\frac{\xi}{R_{\text{NS}}} \right)^4 \simeq \frac{1}{3} \left(\frac{E_{\text{mode}}}{M_{\text{NS}}} \right) \frac{B_{\text{NS}}^2 R_{\text{NS}}^4 \omega^2}{c^3}, \quad (62)$$

where $\mathcal{M} = \frac{1}{2}B_{\text{NS}}R_{\text{NS}}^3$ is the magnetic moment and B_{NS} the polar surface magnetic field. For a mode frequency $\omega \sim 10^4$ Hz, $M_{\text{NS}} = 1.4 M_{\odot}$ and $R_{\text{NS}} = 10$ km, this expression becomes

$$-\left(\frac{dE_{\text{mode}}}{dt}\right)_{\text{MDR}} = 4 \times 10^{40} \left(\frac{E_{\text{mode}}}{10^{44} \text{ ergs}}\right) \left(\frac{B_{\text{NS}}}{10^{15} \text{ G}}\right)^2 \left(\frac{\omega}{10^4 \text{ Hz}}\right)^2 \text{ ergs s}^{-1}. \quad (63)$$

Using either calculation, the rate of dissipation falls by orders of magnitude to accomodate the observed output of the spike – even if the surface field is in the magnetar range.

6. Flare Spectra and Spectral Evolution

6.1. Spectrum of the Hard Initial Spike: An Expanding Pair Fireball

The first part of the August 27 event had a much harder spectrum than the remainder of the outburst. A very hard component $dN/dE \propto E^{-1/2}$ was measured by BeppoSAX during the first 67 seconds, with a much softer power-law component $dN/dE \propto E^{-4.5}$ remaining during the following 128 seconds (Feroci et al. 1999; Paper I). The detection by Konus/Wind of a dramatic drop in the > 250 keV emission following ~ 0.7 sec post-trigger (Mazets et al. 1999) suggests that the very hard spectrum component was mostly emitted during the initial spike.

The large-amplitude fluctuations detected in > 250 keV photons at the end of the hard spike are also remarkable (Mazets et al. 1999). At 0.2 – 0.7 sec after the event’s onset, these fluctuations were more profound in > 250 keV photons than in the 15–250 keV band, and occurred on timescales as short as $\sim 10^{-2}$ s. This behavior is reminiscent of high-redshift, classical gamma-ray bursts (GRBs), in which the light curve is often much smoother at lower energies (Pendleton et al. 1997).

The peak luminosity of the August 27 spike ($L > 4 \times 10^{44}$ ergs s^{-1} ; Mazets et al. 1999) is intermediate, on a logarithmic scale, between a thermonuclear flash and a high-redshift GRB. But we have much more reliable, direct information about its source, SGR 1900+14, than we do about the sources of cosmological GRBs. Thus, detailed studies of the August 27 flare may pay dividends in understanding the more mysterious classical GRB sources, even though the integrated spectrum of the August 27 flare is not typical of a classical GRB.

The volume of the emission region is strongly constrained by the rapid variations in the > 250 keV flux. Although the hard power-law component is detected only up to ~ 700 keV (Feroci et al. 1999), there is no evidence for a high energy cutoff. Therefore, let us

consider the consequences of a source function that extends above an energy $\sim m_e c^2$ in the (relativistically) expanding frame of the outflowing particles and magnetic field that power the hard spike. Pair creation will attenuate the flux above a measured energy $\Gamma m_e c^2$, where Γ is the bulk Lorentz factor of the outflow. Because the photon flux is dominated by high-energy photons ($d\mathcal{N}/dE \propto E^{-1/2}$), one expects copious pair creation, and the luminosity in relativistic pairs is comparable to the photon luminosity. Pairs then make the outflow very thick to scattering, out to a considerable radius

$$R_{\tau=1} \sim \left(\frac{\Delta E \sigma_T}{4\pi \Gamma m_e c^2} \right)^{1/2}. \quad (64)$$

Here, $\Delta E \sim L \Delta t$ is the energy carried by an *individual spike* of peak luminosity L and width Δt . In order for the spike not to be smeared out as the hot shell of ejecta expands to a thickness $\sim R/2\Gamma^2$, one requires $c\Delta t > R_{\tau=1}/2\Gamma^2$, or equivalently

$$\Gamma > \Gamma_{\min} = 7 \left(\frac{L}{10^{43} \text{ ergs s}^{-1}} \right)^{1/5} \left(\frac{\Delta t}{0.01 \text{ s}} \right)^{-1/5}. \quad (65)$$

Most of the dissipation that produces the hard non-thermal spectrum must therefore occur at a large radius,

$$R > R_{\tau=1} \sim 3 \times 10^{10} \left(\frac{L}{10^{43} \text{ ergs s}^{-1}} \right)^{2/5} \left(\frac{\Delta t}{0.01 \text{ s}} \right)^{3/5} \left(\frac{\Gamma}{\Gamma_{\min}} \right)^{-1/2} \text{ cm}. \quad (66)$$

The emission region of the non-thermal spectral component is very large, but comparable to the speed-of-light cylinder of SGR 1900+14 ($cP/2\pi = 2.5 \times 10^{10}$ cm). It sits far enough out that direct synchrotron cooling off the dipole field of the source can be neglected — even if the field lines are combed out into a $\sim R^{-2}$ geometry by the pressure of the escaping particles and radiation. By contrast, the ejecta from the outburst could carry a significant magnetic field. For example, $B \sim R^{-1}$ if Γ grows linearly with radius — as is expected in an expanding fireball which contains a magnetic field but whose pressure is predominantly thermal at the source. Alternatively, inverse-Compton cooling by advected X-ray photons will still be a powerful coolant at a radius (66). The cooling time of a particle of random energy $\gamma_e m_e c^2$ in the bulk frame is $t_{\text{Compton}} \sim \gamma_e^{-1} (\sigma_T L / 4\pi R^2 \Gamma^2 m_e c^2)^{-1}$, and so the ratio of the cooling time to the flow time

$$\frac{t_{\text{Compton}}}{R/c\Gamma} \sim \gamma_e^{-1} \left(\frac{R}{R_{\tau=1}} \right) \left(\frac{\Gamma}{\Gamma_{\min}} \right)^{5/2}. \quad (67)$$

6.2. The Pulsating Tail Spectrum: Temperature Regulation through Photon Splitting

We now consider the temperature of the radiation escaping from a trapped fireball, and compare it with the best (blackbody) temperature fit to the pulsating tail of the August 27 flare. The temperature appears to have remained remarkably constant during the phase of large-amplitude pulsations, even as the X-ray flux continued to decline (Mazets et al. 1999). The best two-component spectral fit (black body + powerlaw) yields $kT_{bb} = 10.8$ keV during interval B (Table 2 of Paper I) and 12.2 keV during interval C (Table 3 of Paper I). These values are consistent with the *minimum* photospheric temperature of a trapped fireball in super-QED magnetic fields, as calculated by TD95.

Near the photosphere, the spectral shape is determined by two coupled processes: Compton scattering and the creation of new photons through splitting $\gamma \rightarrow \gamma + \gamma$ (TD95). The photons flowing out from the base of the trapped fireball are expected to dominate the specific heat and so, in the absence of an extended pair corona, the mean energy per photon will remain approximately constant *outside* the fireball photosphere. Within the outer layers of the optically thick fireball, the photons can maintain a Planckian distribution at temperatures well below the internal fireball temperature of ~ 1 MeV. The mean energy of the escaping photons depends directly on the splitting rate as a function of frequency. In marked contrast with the strong B^6 scaling of the splitting rate in sub-QED magnetic fields, the splitting rate approaches a B -independent value in fields much stronger than B_{QED} ,

$$\Gamma_{\text{sp}}(\omega, B, \theta_{kB}) = \frac{\alpha_{\text{em}}^3}{2160\pi^2} \left(\frac{m_e c^2}{\hbar} \right) \left(\frac{\hbar\omega}{m_e c^2} \right)^5 \sin^6 \theta_{kB} \quad (68)$$

(Adler 1971; Thompson & Duncan 1992). This implies immediately that an E-mode photon propagating a distance $R_{\text{NS}} \sim 10$ km through a super-QED B-field will split if $\hbar\omega > 38 (R_{\text{NS}}/10 \text{ km})^{-1/5}$ keV (TD95; Baring 1995).

Compton scattering becomes strongly anisotropic in a background magnetic field, with a frequency-dependent cross-section. Near the surface of the star, the energy of the first Landau excitation [about $(2B/B_{\text{QED}})^{1/2} m_e c^2$] is much higher than the temperature of the emerging X-rays. In this situation, there is a strong suppression of the E-mode's scattering cross-section: $\sigma_E = (\omega m_e c / e B_0)^2 \sigma_T$ (e.g. Herold 1979). By contrast, the O-mode scatters with a cross-section near Thomson (except for propagation almost parallel to the background field). This suppression of the E-mode scattering opacity greatly increases the radiative transport rate close to the neutron star. One has

$$\frac{\tau_E(T_e)}{\sigma_T(n_{e^+} + n_{e^-})R} = 5\pi^2 \left(\frac{kT_e}{m_e c^2} \right) \left(\frac{B}{B_{\text{QED}}} \right)^2, \quad (69)$$

when the dielectric properties of the medium are dominated by vacuum polarization (Silan'tev & Iakovlev 1980; TD95). First considered as a way to enhance emission from a hydrostatic atmosphere that is confined by gravity at the surface of an ultra-magnetized neutron star (Paczyński 1992; Ulmer 1994; Miller 1995), the suppression of E-mode scattering has potentially more direct applications to radiative transport *across* the confining magnetic field lines of a trapped fireball (TD95).

The two polarization modes are also distinguished by their ability to split. Only the E-mode can split because – when vacuum polarization dominates the dielectric properties of the medium – only the energy and momentum of E-mode photons can be conserved by dividing into two obliquely propagating daughter photons. Splitting occurs predominantly via

$$E \rightarrow O + O, \quad (70)$$

with $E \rightarrow E + O$ having a lower rate (e.g. Berestetskii et al. 1980). When the photon distribution is close to Planckian, net transport out of the E-mode by splitting is suppressed by the inverse process of merging $O + O \rightarrow E$ (TD95). A cascade of photons from high to low X-ray energies cannot occur purely through splitting, as conjectured by Baring (1995), even in magnetic fields as strong as $\sim 10^{16}$ G.

Even in the region where the E-mode is able to stream freely, the O-mode can still undergo many Compton scatterings and relax close to a Bose-Einstein distribution. This permits a very simple generalization of the LTE diffusion formalism to an anisotropic, magnetized plasma at large E-mode scattering depth, in which the photon energy and number fluxes are expressed as linear superpositions of gradients in the temperature T and photon chemical potential μ (TD95). As a result, there is a critical temperature above which the distributions of the E- and O-modes both become thermal, which works out to

$$kT_{\text{sp}} = 11 \left(\frac{R_{\text{NS}}}{10 \text{ km}} \right)^{-1/5} \text{ keV} \quad (71)$$

(eq. [133] in TD95). This value matches well the best fit temperatures for the August 27 event. The mean energy per escaping photon cannot fall below $\sim 2.7kT_{\text{sp}}$, in the absence of new photon creation processes or strong adiabatic cooling.

Now let us consider the spectral variations within each 5.16-s rotation period. The emission is harder at the peaks than in the valleys (see the hardness ratio plots in Fig. 7a of Mazets et al. 1999). A positive correlation between hardness and intensity is expected of thermal emission from an optically thick plasma. Nonetheless, the large-amplitude oscillations show overall an anti-correlation between hardness and intensity (Paper I). A deep trough is present in each rotation cycle after ~ 40 s, and plausibly involves occultation

of the trapped fireball by the neutron star. The spectrum evolves from hard to soft across the trough, which contributes to an overall sawtooth-like pattern in the hardness ratio (see Fig. 1 in Feroci et al. 1999). This hard-to-soft evolution suggests a significant deviation from mirror symmetry in the confining magnetic field with respect to the center of the trough.

7. The Smooth ~ 40 Tail: A Continuously Heated Pair Corona

The giant flares share two main features: an extremely bright, hard, and brief ~ 0.5 -s transient at the onset of the burst; and an extended train of softer, large-amplitude pulses which repeat coherently at the rotational frequency of the star. The initial spike has the properties expected of an expanding, pair-dominated fireball; and, as shown in Paper I, the declining amplitude of the pulsations in the August 27 flare can be well fit by the contracting surface of a trapped fireball.

Nonetheless, this simple picture of a sudden release of thermal energy within the first ~ 1 s, part of which escapes directly and the rest of which remains confined close to the star, does not appear to provide a complete description of the August 27 flare. Within the first ~ 40 seconds, the X-ray flux declines smoothly and shows only a mild modulation at the 5.16-s spin of the source (Figs. 6 and 7 of Paper I). The flux *exceeds* the favored trapped fireball model during this interval (Fig. 3 of Paper I), and the spectral hardness decreases by a factor ~ 1.5 before flattening out after ~ 40 s (Mazets et al. 1999). This behavior was ascribed in Paper I to an extended, pair-dominated corona that scatters and heats the thermal radiation emerging from the inner, trapped fireball (Fig. 5).

This ~ 40 s coronal component of the August 27 flare emitted about 20 percent of the total energy (excluding the hard ~ 0.5 s initial spike; §6.3 of Paper I). At $t \sim 15$ s, the total luminosity was twice the envelope of the trapped fireball, which according to eq. (34) at that time hardly deviates from its initial value $L_X(0) = (1 + \chi)E_{\text{fireball}}/t_{\text{evap}}$. Here $\chi \simeq 3$ is the fireball index, E_{fireball} the initial fireball energy, and $t_{\text{evap}} \simeq 375$ s the time at which the fireball evaporates.

The cooling time of this corona is very short given the high burst luminosity. For an optical depth to scattering $\tau_{es} \gtrsim 1$ (as required by the radiative model discussed below) the cooling time is set by radiative diffusion to a magnitude $\sim \tau_{es}R_{\text{corona}}/c = 10^{-3}(\tau_{es}/10)(R_{\text{corona}}/30 \text{ km})$ s. Thus, the coronal heating must be almost continuous. It could be powered in at least two ways: through a persistent creep of the crust at the heated fracture site, which results in continued shearing of the external

field; or possibly by a coupling of internal shear oscillations to the magnetosphere (§3.2.2). The flare light curve does not provide a simple diagnostic between these alternatives.

7.1. Steady Compton Heating of the O-mode

Why should a continuing release of seismic energy lead to the formation of a distinct scattering atmosphere, instead of merely adding energy to a trapped fireball which forms during the first ~ 0.5 s of a giant flare? We now show that there is a *critical rate* for injection of energy into the trapped fireball, above which the energy becomes trapped before it can leak out radiatively; but below which a steady balance between heating and diffusive radiative cooling is possible. This critical luminosity depends on the nature of the photon source. When double-Compton emission dominates, the answer is given in Thompson (1997). In the present context, photon splitting $\gamma \rightarrow \gamma + \gamma$ is the most effective source of new photons above a critical temperature $T \sim 11$ keV (TD95)

We first summarize the properties of a pair corona with a temperature $kT_e \ll m_e c^2$ in a very strong magnetic field $B \gtrsim B_{\text{QED}}$. A realistic heating mechanism involves electrostatic acceleration of the pairs through a turbulent cascade of interacting Alfvén waves: the current density is driven just above the value that can be supported self-consistently by the available particles, and a displacement current is induced parallel to the background magnetic field (Thompson & Blaes 1998).

The pairs cool primarily by Compton upscattering the O-mode, due to its much larger cross section. Although at large scattering depth radiation diffuses fastest via the E-mode, the orthogonal O-mode will be regenerated⁸ by scattering (with cross section $\tau_{EO} \simeq \tau_E$; Mészáros 1992) and by splitting (TD95; Miller 1995). Moreover, in some circumstances the optical depth may be too small to allow effective mode transfer $O \rightarrow E$ by scattering. (Conversion of the O-mode to the E-mode does not occur by splitting, except at enormous optical depths where the plasma dominates the dielectric properties of the medium.)

In the following discussion, we will assume that the electrostatically heated pairs are sub-relativistic and pinned in the lowest Landau level. Indeed, at the very high compactness ($\ell \equiv L_X \sigma_T / 4\pi m_e c^3 R_{\text{NS}} \sim 10^6$) characteristic of the August 27 smooth tail, the pairs will equilibrate at a temperature close to that of the O-mode photons. Since the effective

⁸Indeed, the inability of high energy O-mode photons to split, combined with their rapid Compton heating by pairs, provides a mechanism for generating the non-thermal X-ray spectra of SGRs in their quiescent (non-bursting) state.

temperature of the photons is $kT_O \sim 10 - 20$ keV, the spectral distribution of Comptonized photons will have an exponential cutoff $F_\nu \propto \exp(-h\nu/kT_e)$ at high energies $h\nu \gtrsim kT_e$.

The question which we address here is: what is the range of temperature for which the pair plasma is stable to an upward excursion in the density $n_{e^+} + n_{e^-} \simeq 2n_{e^+}$ of electrons and positrons? An accompanying increase in the pair temperature T_e forces a runaway of the pair density (due to the higher flux of Comptonized photons above the pair-creation threshold $h\nu \sim m_e c^2$). This runaway is inevitable if the pair plasma is in local thermodynamic equilibrium (TD95).

If, instead, T_e decreases when n_{e^+} increases, then a stable balance between electrostatic heating and diffusive photon cooling is possible. Then the distribution functions of E-mode and O-mode are both approximately Wien. Such a steady balance requires a continuous source of O-mode photons, which can be provided either internally by splitting the E-mode, or externally by scattering incident E-radiation to the O-mode.⁹ Splitting can be expected to dominate where the magnetic field is stronger than B_{QED} ; but an external source of E-mode photons is necessary in a more extended corona around a bursting magnetar. We consider each case in turn.

7.2. Equilibrium Temperature of the Corona

We first consider the equilibrium temperature of the corona, given a steady balance between the rate L_{corona} at which the pairs are electrostatically heated, and radiative transport out of the magnetosphere. The result depends on the mechanism by which radiative transport occurs (through the E-mode or the O-mode). We idealize the corona as a sphere of radius R .

If the source of photons lies below the corona – i.e. in the form of a cooling trapped fireball – then photons diffuse into the corona predominantly via the E-mode, before being converted to the O-mode and heated. One deduces that $\tau_{EO} \gtrsim 1$ (and that energy is also transported *out* of the corona through the E-mode). In addition, the scattering depth to the O-mode is very large,

$$\frac{\tau_O}{\tau_{EO}} \sim \frac{1}{5\pi^2} \left(\frac{B}{B_{\text{QED}}} \right)^2 \left(\frac{kT_E}{m_e c^2} \right)^{-2}. \quad (72)$$

⁹Double Compton scattering of the O-mode — $O + e^\pm \rightarrow O + O + e^\pm$ — is an effective source of new photons only at larger scattering depths than are needed to convert the E-mode.

(Here T_E is the temperature of the *external* photon source, and we have made use of eq. 69.) Fresh O-mode photons are rapidly Compton heated up to a Wien distribution with temperature $T_O \simeq T_e$ and mean energy per photon $3kT_e$. Furthermore, the E-mode and O-mode photons are in equilibrium at large τ_{EO} , and one has $T_E \simeq T_e$, $n_E \simeq n_O$.

The balance between heating and diffusive radiative cooling becomes

$$\frac{L_{\text{corona}}}{4\pi R^2 c} = \frac{3kT_E n_E}{3(2n_{e+}\sigma_E(T_E)R)} \quad (73)$$

As just described, such a steady balance requires that photon creation be too slow to establish local thermodynamic equilibrium. The densities of photons and pairs are then related by

$$\frac{n_{e+}}{n_{e+}(LTE)} \simeq \frac{n_O}{n_O(LTE)}. \quad (74)$$

The corresponding LTE densities are

$$2n_{e+}(LTE) = \frac{(m_e c)^3}{\hbar^3 (2\pi^3)^{1/2}} \left(\frac{B}{B_{\text{QED}}} \right) \left(\frac{kT_e}{m_e c^2} \right)^{1/2} \exp\left(-\frac{m_e c^2}{kT_e}\right), \quad (75)$$

and

$$2n_O(LTE) = n_O(LTE) + n_E(LTE) = 0.244 \left(\frac{kT_e}{\hbar c} \right)^3 \quad (76)$$

at temperature T_e . The equilibrium temperature is then determined from eqs. (69) and (73),

$$\frac{L_{\text{corona}}}{10^{34} \text{ ergs s}^{-1}} = \left(\frac{kT_e}{m_e c^2} \right)^{3/2} \exp\left(\frac{m_e c^2}{kT_e}\right) \left(\frac{B}{B_{\text{QED}}} \right) \left(\frac{R}{10 \text{ km}} \right). \quad (77)$$

The temperature corresponding to the brightest, short SGR outbursts ($\sim 10^{42}$ ergs s^{-1}) in super-QED fields ($B/B_{\text{QED}} \sim 10$) is $kT_e \sim 25$ keV, which increases only to ~ 50 keV at $L_{\text{corona}} \sim 10^{38}$ ergs s^{-1} (Fig. 6).

It is also possible that the photon source is *internal* to the corona (e.g. splitting). The corona can then maintain a much lower scattering depth while cooling diffusively through the O-mode – without any need for converting photons back to the E-mode. In this case, the balance between heating and cooling becomes

$$\frac{L_{\text{corona}}}{4\pi R^2 c} \sim \frac{3kT_O n_O}{3(2n_{e+}\sigma_T R)}, \quad (78)$$

since $\sigma_O \sim \sigma_T$ after averaging over angles. The equilibrium temperature is now determined by

$$\frac{L_{\text{corona}}}{10^{34} \text{ ergs s}^{-1}} = 44 \left(\frac{kT_e}{m_e c^2} \right)^{7/2} \exp\left(\frac{m_e c^2}{kT_e}\right) \left(\frac{B}{B_{\text{QED}}} \right)^{-1} \left(\frac{R}{10 \text{ km}} \right). \quad (79)$$

Notice the different dependence on both T_e and B/B_{QED} . In this case, the temperature corresponding to $L_{\text{corona}} \sim 10^{42}$ ergs s^{-1} in a magnetic field $\sim 10 B_{\text{QED}}$ is slightly lower, $kT_e \sim 20$ keV, increasing to $kT_e \sim 30$ keV at $L_{\text{corona}} \sim 10^{38}$ ergs s^{-1} (Fig. 6).

7.3. Critical Luminosity: Photons Created by Splitting

We now look for the maximum energy input to the corona that allows a steady balance between heating and diffusive cooling. The key criterion is that the equilibrium pair density n_{e^+} be smaller than the LTE value (75).

Photon splitting will occur within the bulk of the corona. We can assume that photon transport out of the corona is through the O-mode, because splitting converts the E-mode to the O-mode (but not the reverse). As a result, transport cannot occur self-consistently via the E-mode. A high temperature $kT_O \gtrsim 20$ keV is needed to generate sufficient pairs to scatter the O-mode back to the E-mode ($\tau_{OE} \gtrsim 1$); but because this temperature is well above the critical value (~ 11 keV) where splitting is rapid, the transport of E-mode photons will be limited by splitting, $L_{\text{corona}}/4\pi R^2 c \sim 3kT_E n_{EC}/\Gamma_{\text{sp}} R$. In this situation, it would not be possible to maintain a steady balance between the creation and the outward diffusion of photons, because the rate of creation of photons $\dot{N}_\gamma \sim 4\pi n_E R^3 \Gamma_{\text{sp}}$ would exceed $L_{\text{corona}}/3kT_E$ by a factor $\sim (\Gamma_{\text{sp}} R/c)^2 \gg 1$.

Instead, the radiative flux out of the corona is carried by the O-mode. A steady balance between photon creation and loss requires that each diffusing O-mode photon have a substantial probability ($\sim \frac{1}{2}$) of converting to the E-mode and splitting.¹⁰ Thus $\tau_{EO}\tau_O \sim 1$, which corresponds to

$$5\pi^2 \left(\frac{kT_e}{m_e c^2} \right)^2 \left(\frac{B}{B_{\text{QED}}} \right)^{-2} \tau_O^2 \sim 1. \quad (80)$$

But

$$\tau_O \sim (2n_{e^+})\sigma_T R = 1.5 \left(\frac{n_{e^+}}{n_{e^+}(\text{LTE})} \right) \left(\frac{L_{\text{corona}}}{10^{42} \text{ ergs s}^{-1}} \right)^{-1} \left(\frac{kT_e}{20 \text{ keV}} \right)^4 \left(\frac{R}{10 \text{ km}} \right)^2 \quad (81)$$

(making use of eqs. [75] and [79]). The bound $n_{e^+} < n_{e^+}(\text{LTE})$ then implies, together with

¹⁰Once again, we must assume that the photon density is well below the black body value at temperature T_O to obtain a steady balance between heating and cooling. Thus, the inverse process of photon merging can be neglected.

eq. (80),

$$L_{\text{corona}} < L_{\text{corona}}(\text{max}) = 4 \times 10^{41} \left(\frac{B}{B_{\text{QED}}} \right)^{-1} \left(\frac{kT_e}{20 \text{ keV}} \right)^5 \left(\frac{R}{10 \text{ km}} \right)^{-2} \text{ ergs s}^{-1}. \quad (82)$$

A stable balance between heating and diffusive cooling is possible *below* the luminosity $L_{\text{corona}}(\text{max})$. In such an equilibrium, the electron temperature is strongly buffered and remains close to 20 keV as L_{corona} varies by a few orders of magnitude around $\sim 10^{42}$ ergs s^{-1} (eq. [79]). The right side of eq. (82) scales as $\sim R$ in a dipolar magnetic field.

This equilibrium between heating and cooling is steady, as it is straightforward to check. A rise in n_{e^+} implies an increase in τ_O , which must be compensated by a decrease in τ_{EO} to maintain the relation $\tau_O \tau_{EO} \sim 1$ (eq. 80). By contrast, when the fireball is in local thermodynamic equilibrium, an increase in n_{e^+} is directly tied to an increase in T . In such a situation, continuing energy input will force a runaway increase in the energy density to a trapped fireball (TD95).

7.4. Critical Luminosity: External Source of Photons

Now consider the case where the corona is sufficiently extended that the magnetic field is weaker than B_{QED} , and photon splitting can be neglected over most of its volume. Diffusive cooling now occurs through the E-mode, and a steady balance between heating and cooling fixes the electron temperature through expression (73). Given a source \dot{N}_E^{ex} of fresh E-mode photons (of temperature T_E^{ex}) escaping from the trapped fireball, the optical depth through the corona is fixed. In the regime of interest, $\tau_{EO} > 1$, and the soft fireball photons are heated by only a fraction $\sim \tau_{EO}^{-1}$ of the coronal input L_{corona} : the equilibrium pair temperature is fixed by energy conservation.

$$\dot{N}_E^{\text{ex}} \times 3(T_E - T_E^{\text{ex}}) = \frac{L_{\text{corona}}}{\tau_{EO}}. \quad (83)$$

(We neglect the difference between the mean energy per photon in the blackbody and Wien distributions. This expression is approximately valid even for low τ_{EO} , where only a fraction $\sim \tau_{EO}$ of the fireball luminosity is captured by the corona.) Combining this relation with $L_{\text{corona}} = (3kT_E)\dot{N}_E^{\text{ex}}$ gives

$$\tau_{EO} \simeq \left(1 - \frac{T_E^{\text{ex}}}{T_E} \right)^{-1} = O(1). \quad (84)$$

At the high luminosities of SGR outbursts, the pairs in the outer corona equilibrate to a temperature only slightly different from that of the heated O-mode photons. During

repeated scatterings, the mean energy per photon exponentiates as e^y , where the Compton parameter is

$$y \sim 4\tau_O^2 \frac{k(T_e - T_O)}{m_e c^2}. \quad (85)$$

In equilibrium,

$$y = \ln \left(1 + \frac{L_{\text{corona}}}{L_{\text{fireball}}} \right), \quad (86)$$

which implies

$$\frac{T_e}{T_O} - 1 \sim \frac{y}{4\tau_O^2} \left(\frac{m_e c^2}{kT_O} \right) \ll 1. \quad (87)$$

We can now determine the critical luminosity below which a steady balance between heating and cooling is possible. One has, from equations (73) and (75),

$$\tau_{EO} \sim (2n_{e^+})\sigma_E(T_E)R = 1.5 \left(\frac{n_{e^+}}{n_{e^+}(LTE)} \right) \left(\frac{L_{\text{corona}}}{10^{42} \text{ ergs s}^{-1}} \right)^{-1} \left(\frac{kT_e}{20 \text{ keV}} \right)^4 \left(\frac{R}{10 \text{ km}} \right)^2. \quad (88)$$

This expression is very similar to (81), with the distinction that diffusive transport is through the E-mode instead of the O-mode. As a result, T_e is slightly higher than in the case where fresh photons are created by splitting (but is still strongly buffered through eq. [77]). The critical luminosity is determined by setting $n_{e^+} < n_{e^+}(LTE)$:

$$L_{\text{corona}} < L_{\text{corona}}(\text{max}) = 1.5 \times 10^{42} \left(1 - \frac{T_E^{\text{ex}}}{T_E} \right) \left(\frac{kT_e}{20 \text{ keV}} \right)^4 \left(\frac{R}{10 \text{ km}} \right)^{-2} \text{ ergs s}^{-1}. \quad (89)$$

As before, this equilibrium is steady as long as the densities of O-mode and (heated) E-mode photons lie below the blackbody value at temperature $T_e \simeq T_O$. That is because a rise in n_{e^+} increases τ_{EO} , and hence *reduces* the equilibrium (Wien) temperature to which the escaping fireball photons will be heated (eq. [83]).

After the coronal heating rate L_{corona} drops below the luminosity of the cooling fireball, this pair atmosphere evaporates and the scattering photosphere contracts to the outer boundary of the trapped fireball, where the opacity is dominated by ion-electron plasma (TD95). This provides an explanation for the flattening of the light curve simultaneously with the appearance of large-amplitude oscillations. We outline the effects of the strong magnetic field on this Compton corona in the next section.

7.5. Very High Current Densities

In the preceding, we have assumed that the pairs are heated electrostatically by a fluctuating current, and derived the critical heating rate above which the pair-photon plasma runs away to local thermodynamic equilibrium. There is, similarly, a critical current density J above which photons will remain trapped in the current-carrying region. The energy density of the photons exponentiates, thereby creating a pair plasma in local thermodynamic equilibrium.

The optical depth to the O-mode through the current-carrying charges is

$$\tau_O \sim (n_{e^-} + n_{e^+})\sigma_T R \sim \frac{J}{eV}\sigma_T R, \quad (90)$$

where R is the size of the current-carrying region. In a pure pair plasma, with equal numbers of charges moving in opposite directions along the magnetic field lines, the mean frequency shift per scatter is second order in the drift speed V of the current carriers, $\Delta\nu/\nu \sim (V/c)^2$. In equilibrium, the temperature of the photons and (1-dimensional) pairs is

$$kT_O \simeq \left(\frac{V}{c}\right)^2. \quad (91)$$

When $\tau_O > 1$, each O-mode photon undergoes $\sim \tau_O^2$ scatterings, and the Compton parameter

$$y \sim \tau_O^2 \left(\frac{V}{c}\right)^2 \sim \left(\frac{J\sigma_T R}{ec}\right)^2 \quad (92)$$

depends only on the current density J and the size R of the ‘corona’. However, T_O is strongly buffered by pair creation and annihilation (§7.2). Thus, above a critical current density J , the scattering depth becomes too large to allow the photons to diffuse out before their *number* and energy density multiplies. For example, in the case where new photons are created by splitting, the critical current density corresponds to an optical depth τ_O equal to (80).

7.6. Alternative Models for the Smooth Tail

Let us consider two alternative explanations for the smooth tail: a steady increase in the ion-electron loading at the fireball surface; and neutrino cooling. Each of these alternatives fails in some manner.

The portion of the neutron star surface that is exposed to the hot fireball will drive a super-Eddington wind as the fireball begins to contract (TD95). This could force a

steady increase in the density of ions and electrons, supported above the surface by the photon pressure. At high enough temperatures the radiative flux from the surface of the fireball is fixed self-consistently by the opacity of this suspended matter (TD95): $\frac{1}{2}\sigma_{SB}T_{eff}^4 \simeq F_{\text{edd}} [\sigma(T_{eff}, B)/\sigma_T]^{-1} \varepsilon_{ion} (\ell/R_{\text{NS}})^{-1}$. Here, F_{edd} is the Eddington flux calculated with the Thomson cross-section; $\sigma(T_{eff}, B)/\sigma_T = 5\pi^2 [kT/(\hbar eB/m_e c)]^2$ is the scattering opacity in the strong background magnetic field; ε_{ion} is the ion density compared with the maximum that can be supported against gravity; and ℓ is the thickness of the ion-electron layer at the photosphere. As the fireball contracts and ℓ increases (due to the increasing exposure of heated crust) the radiative flux decreases as $\ell^{-2/3}$ and the effective temperature decreases as $T_{eff} \propto \ell^{-1/6}$. Although this variant offers a nice explanation for the decrease in radiative flux and temperature during the smooth ~ 40 s tail, it has difficulty accomodating the *contraction* of the photosphere that is required by the transition to large-amplitude pulsations.

Neutrino cooling does not change the lightcurve of a homogeneous fireball in the manner needed to explain the ~ 40 -s smooth tail (Figs. 4a, 4b). The fireball could, of course, have two components, one of which has a much higher temperature T_{high} and emits neutrinos much more rapidly than the cooler component. Then $T_{high} \propto t^{-1/5}$ and the radiative flux from the contracting surface of the fireball decreases as¹¹ $F \propto T_{high}^{5/2} \propto t^{-1/2}$. However, it is difficult to understand why the energy radiated from the higher temperature component should be much smaller (by a factor ~ 20), even while it covers a much larger volume (so as to explain the absence of large-amplitude pulsations).

8. The Four-Peaked Repetitive Pattern: Collimated X-ray Jets

A dramatic four-peaked pattern emerged in the August 27 light curve at ~ 40 s following the burst trigger. This pattern repeated with the 5.16-s rotation period of the neutron star. At times, the flux varied by more than an order of magnitude from peak to trough. However, there is no significant break in the pulse-averaged light curve during the appearance of the four-peaked pattern (Fig. 4 of Paper I), which indicates that the beamed flux is redistributed over the pulse period.

The phase stability of the X-ray jets suggests that they are tied to surface features on the neutron star. Indeed, it has previously been argued that the radiative flux out of a trapped fireball could become significantly collimated along the magnetic field lines that open out to a few neutron star radii (TD95). Figure 7 outlines the basic geometry. A

¹¹This applies when the higher Landau levels are populated; eq. (89) of TD95.

$10^{14} - 10^{15}$ G magnetic field is certainly strong enough: its pressure exceeds the radiative momentum flux by some 9-10 orders of magnitude. In this picture, the approximate ~ 1 -s periodicity apparent in the four-peaked pattern is a chance byproduct of the location of the outburst, and the multipolar structure of the neutron star’s surface magnetic field (Paper I; Fig. 8). The difference in the number of sub-pulses observed within each rotation during the August 27 and March 5 giant flares, can then be ascribed to a difference in the number of xray jets. The most plausible geometry for each jet is a fan beam, which is swept past the line of sight once or twice by the rotation of the star. Figure 8 illustrates one possible geometry for each event, where each fan beam is observed twice as two separate sub-pulses.

The large disparity between the scattering cross sections of the E-mode and O-mode is the underlying reason for collimation. In addition, the scattering opacity of the E-mode rises rapidly with radius, $\sigma_E \propto B^{-2} \propto R^6$ in a dipole geometry. As a result, radiative transport across the magnetic field lines is concentrated close to the neutron star surface (TD95). The trapped fireball heats a thin outer skin of the neutron star crust, and as the fireball contracts the cooling flux of X-rays drives matter off its surface (Ibrahim et al. 2000). This ablated material is easily suspended by Compton scattering¹² in the magnetosphere, where it remains confined.

The rapid growth of the E-mode opacity then provides a mechanism for self-collimation: the E-radiation can escape only by pushing the suspended matter to the side (Fig. 7). The ion-electron photosphere of the fireball is congruent with a set of magnetic field lines, as the result of pressure gradient forces along the field. (The cooling time exceeds the sound-crossing time of the fireball by a factor of a million.) This means that the collimation occurs primarily along magnetic field lines that open out beyond the electron-ion photosphere.

The width of each X-ray jet depends on the amount of matter advected with the photons, and can be estimated as follows. A significant fraction of the E-mode flux near the E-mode photosphere is converted to the O-mode by photon splitting (TD95). Mode changing also occurs via non-resonant Compton scattering near the E-mode photosphere (Miller 1995; TD95), as well as by resonant Compton scattering near the ion cyclotron line (Thompson 2000). The O-mode photons have scattering cross-sections near Thomson; i.e., the scattering of O-mode photons is *not* significantly suppressed by the strong magnetic field. Thus, the energy flux injected into the O-mode near the neutron star surface is tremendously super-Eddington, both due to the large luminosity $L_O \sim \frac{1}{2}L_X$ and the small

¹²By non-resonant scattering off the O-mode, or by resonant scattering at the ion cyclotron fundamental (which lies in the X-ray range in $\sim 10^{14} - 10^{15}$ G magnetic fields; Ibrahim et al. 2001).

beaming angle $\Delta\Omega_{\text{jet}}$:

$$F_O = \frac{L_O}{R_{\text{NS}}^2 \Delta\Omega_{\text{jet}}} \sim 3 \times 10^3 \left(\frac{L_X}{10^{42} \text{ ergs s}^{-1}} \right) \left(\frac{\Delta\Omega_{\text{jet}}}{4\pi} \right)^{-1}. \quad (93)$$

The O-mode flows hydrodynamically along the magnetic field even in the presence of a tiny amount of matter, which can generate a large scattering depth along the magnetic field:

$$\tau_{\parallel}(R_{\text{NS}}) \sim \frac{\dot{M}\sigma_T}{R_{\text{NS}}\Delta\Omega_{\text{jet}}m_p c} = \left(\frac{\dot{M}c^2}{L_O} \right) \left(\frac{L_O}{L_{\text{edd}}} \right) \left(\frac{GM_{\text{NS}}}{R_{\text{NS}}c^2} \right) \left(\frac{\Delta\Omega_{\text{jet}}}{4\pi} \right)^{-1} \quad (94)$$

The resulting radiatively-driven outflow is probably relativistic (§6.4 of TD95). Indeed, it quickly becomes relativistic if the photons dominate the specific heat and their expansion is adiabatic. The conserved enthalpy per photon can be expressed in terms of the (bulk frame) photon density n_γ and the bulk Lorentz factor γ as $\gamma(\hbar c)n_\gamma^{1/3} \sim kT(R_{\text{NS}})$; and the rate at which photons are carried through the jet is

$$\dot{N}_\gamma = (\gamma n_\gamma) \Delta\Omega_{\text{jet}} R^2 c \sim \left[\frac{T(R_{\text{NS}})}{\hbar c} \right]^3 R_{\text{NS}}^2 \Delta\Omega_{\text{jet}} (R_{\text{NS}}) c. \quad (95)$$

Combining these two expressions gives

$$\gamma \sim \left(\frac{\Delta\Omega_{\text{jet}} R^2}{\Delta\Omega_{\text{jet}}(R_{\text{NS}}) R_{\text{NS}}^2} \right)^{1/2}, \quad (96)$$

which is $\gamma \sim R/R_{\text{NS}}$ in spherical geometry but

$$\gamma \sim \left(\frac{R}{R_{\text{NS}}} \right)^{3/2} \quad (97)$$

in an outflow that is channeled along a dipolar magnetic field¹³.

Photons travelling along field lines, with the angle between wavevector \mathbf{k} and \mathbf{B} satisfying $\theta_{\mathbf{kB}} < (\hbar\omega/m_e c^2)^{1/2} (B/B_{\text{QED}})^{-1/2}$, experience strong suppression of photon scattering even in the O mode (e.g. Mészáros 1992). Inside this wavevector cone, the O and E photon eigenstates are nearly circularly polarized, with opposing helicities, rather than linearly polarized as at more oblique propagation angles. However, this cone is very narrow near the surface of the star: $\theta_{\mathbf{kB}} < 0.05 B_{15}^{-1/2} (\hbar\omega/30 \text{ keV})^{1/2}$ radians. In the zone where the jet outflow is accelerated, just above the stellar surface, the O-mode specific intensity is nearly isotropic, and almost all photons propagate outside the cone.

¹³In this geometry, the cross-sectional area of a flux bundle increases as $\sim R^3$.

As the matter accelerates and expands, the optical depth through it drops off. Let us estimate the radius R_τ where the matter and photons decouple, under the assumption that $\theta_{\mathbf{kB}} \ll 1$ at this radius in the bulk frame. This decoupling radius must be smaller than the maximum radius of the confining magnetic field lines ($\theta_{\text{jet}}^{-2} R_{\text{NS}}$ in a dipole geometry; Fig. 7):

$$\frac{R_\tau}{R_{\text{NS}}} < \theta_{\text{jet}}^{-2} = \frac{\pi}{\Delta\Omega_{\text{jet}}}. \quad (98)$$

To reach a radial path of polar angle θ and escape, the advected photons must diffuse through an angle $\sim \frac{1}{2}\theta$ from the direction of the bulk streaming (which is tangent to the dipolar magnetic field). Thus the photons must diffuse a transverse distance $\Delta R_\perp \sim \frac{1}{2}\theta R$, which corresponds to an optical depth

$$\tau_\perp \sim \frac{n_e(R)}{\gamma} \sigma_T \Delta R_\perp. \quad (99)$$

The diffusion time $\tau_\perp R_\perp/c$ must be shorter than the radial flow time $R/\gamma c$, and we deduce

$$n_e(R) \left(\frac{1}{2}\theta\right)^2 \sigma_T R < 1. \quad (100)$$

Making use of eqs. (94) and (99), this becomes

$$\frac{R_\tau}{R_{\text{NS}}} \sim \frac{\Delta\Omega_{\text{jet}}(R_{\text{NS}})\tau_\parallel(R_{\text{NS}})}{4\pi}. \quad (101)$$

Combining this result with eq. (98), we find that the narrowness of the jet at its base *increases* increases with the optical depth:

$$\frac{\Delta\Omega_{\text{jet}}(R_{\text{NS}})}{4\pi} < \frac{1}{2\tau_\parallel^{1/2}(R_{\text{NS}})} \quad (102)$$

Further collimation can occur when the escaping X-rays cross the surface of the electron cyclotron resonance, which sits at a distance $R/R_{\text{NS}} = 6.7 (\hbar\omega/40 \text{ keV})^{-1/3} (B_{\text{NS}}/10^{15} \text{ G})^{1/3}$ from a neutron star with polar field B_{NS} . During an SGR outburst, the matter suspended and confined at this radius can easily generate a large *Thomson* optical depth. This material is constrained to move along the magnetic field (the magnetic pressure greatly exceeds the radiative energy flux even at such a distance), and so its angular distribution will reflect the multipolar structure of the magnetic field near the stellar surface. However, in the persistent emission, which has a flux well below Eddington, the X-ray pulse profile will be strongly modified by resonant cyclotron scattering off magnetospheric currents (at either the electron or ion resonances: Thompson et al. 2001).

9. Conclusions

The August 27 giant flare provides a Rosetta stone for SGR 1900+14, just as the March 5 giant outburst did for SGR 0526-66. These two remarkable events share very similar peak luminosities, energies, and morphologies, which suggests in turn that these two SGR sources are fundamentally alike.

In the context of the magnetar model, we have discussed the mechanism by which such a giant flare may be triggered, and the physical processes operating in each of the three principal phases of the August 27 flare: the initial ~ 0.4 sec hard spike; the intermediate smooth ~ 40 sec tail, and the final phase of large-amplitude pulsations that displays a striking four-peaked pattern. In the process, we have refined physical arguments that point to an external (dipole) magnetic field stronger than $\sim 10^{14}$ G in SGR 1900+14, and an even stronger $\sim 10^{15}$ G internal (toroidal) field which is the basic energy source for repeated flare activity.

9.1. Physics of giant flares

1. In the flare mechanism proposed here, most of the potential energy that powers a giant flare is stored before the event in the magnetic field of the deep crust and liquid stellar interior (TD95). This slowly-evolving field strains the crust from below. The brittle crust acts as a gate for the catastrophic release of energy. The elastic energy released in the crust is *smaller* than the available magnetic energy by a factor $\sim B^2/4\pi\mu$, where B is the field in the stellar interior and μ the crustal shear modulus, and by appropriate geometrical factors (§3.1).

2. When the internal magnetic field is strongly wound, its stored energy can be rapidly communicated to the stellar exterior via a propagating fracture, involving a rotational deformation of a patch of the crust (§3.2). Such a motion of the neutron star crust can create tangential discontinuities in the magnetic field, and thereby induce dissipation in three distinct zones. First, it induces strong magnetic shear in parts of the magnetosphere, which can rapidly damp through reconnection and conversion to high frequency Alfvén waves; second, a torsional oscillation of the magnetized core is excited (along with an accompanying toroidal deformations of the crust which involve less energy); and third, static current sheets are excited deep in the crust.

3. The damping of an internal shear mode by a flux of Alfvén waves into the magnetosphere has been further quantified. In the case of a large-scale mode with harmonic $\ell \lesssim R_{\text{NS}}/\Delta R_\mu$ (eq. 18), the equilibrium energy stored in a trapped magnetospheric Alfvén

mode is greatly suppressed with respect to the exciting internal mode (eq. [33]). This implies strong lower bounds on the poloidal magnetic field ($B \gtrsim 10^{15}$ G) and internal mode energy $\delta E_{\text{elas}} \gtrsim 10^{44}$ ergs) needed to power the extreme peak luminosity of the initial hard spike (§5.2). We also make a critical comparison of our results with the vibrating neutron star model of Ramaty et al. (1980), and review why an internal f - or p -mode couples even more weakly to the magnetosphere than an internal shear mode.

4. The contracting photosphere of a very hot ($T \sim 1$ MeV) confined fireball provides an excellent fit to the envelope of the 1998 August 27 giant flare after ~ 40 s, and accounts for the rapid final drop in flux (Paper I). We show in §4 that the fireball probably formed hotter in its center than at its edge, because the observed flux diminished faster than it would for a homogeneous, spherical fireball.

5. The light curve appears not to be perturbed by neutrino cooling (Figs. 4a, 4b), which implies an upper bound to the fireball temperature of $T \lesssim T_{\text{max}} = 0.8$ MeV. This in turn provides a conservative lower bound to the volume and magnetic moment of the confining magnetic field. The August 27 outburst alone implies a strict lower bound $\mu > 2.4 \times 10^{31} (E/10^{44} \text{ ergs}) (T/T_{\text{max}})^{-2} \text{ G-cm}^3$. However, two considerations suggest that the net dipole moment is several times larger: the inferred number $\sim 10^2$ of giant outbursts over the history of the source; and the absence of a measureable change at the ~ 10 percent level in the long-term spindown of SGR 1900+14 (Woods et al. 1999; Thompson et al. 2000).

6. The smooth ~ 40 -sec tail of the 27 August flare is somewhat harder than the ensuing large-amplitude pulsations. During this intermediate phase, the modest flux variations do not repeat coherently with rotational phase; and the X-ray flux is significantly higher than predicted by the trapped fireball model which fits observations after ~ 40 sec. In Paper I, we ascribed this excess hard flux to Compton heating by an extended pair photosphere, driven by a persistent seismic excitation of the neutron star. In this paper, we have quantified the behavior of a pair corona in a magnetic field stronger than B_{QED} . Cooling occurs primarily by Compton heating of the O-mode. We defined a critical coronal luminosity (eqs. 82 and 89) below which a steady balance between electrostatic heating and diffusive radiative cooling is possible. This luminosity is $O(10^{42} \text{ ergs s}^{-1})$, which is comparable to the observed output from SGR 1900+14 during the smooth tail. A magnetar flare could inject energy into the magnetosphere at a much higher rate than this critical level. Indeed, the flux of the prompt, hard spike exceeds this minimum luminosity, giving direct evidence that energy was liberated fast enough to form a trapped fireball at the onset of the August 27 flare.

7. The best fit black body temperature is stable during the period of large-amplitude

pulsations (Mazets et al. 1999; Paper I) and agrees well with the value $kT_{\text{sp}} \simeq 11$ keV at which photon splitting freezes out (eq. [180] in TD95).

8. We propose that the large-amplitude pulsations are due to a collimated flux of X-rays from the base of the trapped fireball, moving along extended magnetic field lines (see also TD95; Feroci et al. 2001). Collimation of the E-mode is provided by the rapid increase in its scattering opacity with distance from the stellar surface, $\sigma_E(B) \propto B^{-2} \propto R^6$. The O-mode flows hydrodynamically even in the presence of a small flux of advected ions (and neutralizing electrons), $\dot{M}c^2/L_O \lesssim (L_O/L_{\text{edd}})^{-1}(GM_{\text{NS}}/c^2)^{-1}$. Energy can be released in both polarization modes at comparable rates. The width of the X-ray ‘jet’ can be related directly to the flux of advected matter. The collimation becomes finer as the matter flux increases, because the radiation-hydrodynamical flow must extend to larger radius before the photons and matter can decouple.

9. We have quantified some physical mechanisms that could generate the persistent, hard spectral component of the August 27 flare. In particular, the burst spectrum is harder during dips, which points to acceleration of non-thermal particles or direct Comptonization by large-amplitude Alfvén waves in an extended corona.

9.2. Evidence for Magnetars: Field Strength Estimates

One of the principal goals of this paper is to set more model-independent (lower) bounds on the magnetic field in the flaring SGR sources. Several observational properties of these sources directly require magnetic fields stronger than $\sim 10^{14}$ G (the dipole component) to $\sim 10^{15}$ G (the internal toroidal field, and higher multipoles).

1. The estimated output of $\sim 10^{47}$ ergs in giant flares over the active history of a flaring source corresponds to a r.m.s. magnetic field stronger than $\sim 10^{15}$ G (§2.2).

2. The observed lightcurve of the August 27 flare can be well fit by the cooling of a ‘trapped fireball’ (Feroci et al. 2001). The confinement of a substantial fraction of the outburst energy [$\sim (1 - 3) \times 10^{44}$ ergs] in a pair-photon plasma close to the source, which cools gradually over ~ 300 seconds, implies a lower bound $\sim 10^{14}$ G to the external dipole field (TD95). This argument is refined in §5.1, taking into account the fit of the August 27 flare light curve to the contracting surface of a trapped fireball (Paper I), and the restrictions on the size of the fireball from bulk neutrino-pair cooling. In addition, the intermediate ~ 40 smooth tail in the August 27 flare provides evidence that the seismic output of the source can exceed $\sim 10^4 L_{\text{edd}}$ for a limited time.

3. The extreme peak luminosity of the initial spike ($3 - 10 \times 10^6 L_{\text{edd}}$: Fenimore et al. 1996; Mazets et al. 1999) can be powered through a sudden readjustment of a magnetic field stronger than $\sim 10^{14}$ G (§5.2), especially if this readjustment involved a fracture of the neutron star crust and the formation of regions of strong magnetic shear. Such a violent event would also deposit energy into internal shear modes (including a torsional Alfvén wave in the liquid core and standing shear waves in the rigid crust). We have considered separately the damping of these internal oscillations via a coupling to the magnetosphere. Even under the most optimistic assumptions about the rate at which an external torsional mode is converted to radiation, the observed peak luminosity of the giant flares can barely be supplied if the surface field is $\sim 10^{14}$ G, and cannot be supplied if it is much weaker. The luminosity of the pulsating tail, $L/L_{\text{edd}} \lesssim 10^4$, is consistent with the suppression of the electron scattering opacity of the E-mode radiation near the strongly magnetic surface of a trapped fireball. In the context of the SGR sources, this effect was first discussed by Paczyński (1992), under the assumption that the radiation is released from the cooling surface of a magnetar. However, the physical effect is in fact much cleaner if radiative transport occurs *across* the confining magnetic field lines of a trapped fireball.

It is also worth re-evaluating other arguments for strong magnetic field, in the light of recent observations:

4. The long 8-s spin period of SGR 0526-66, combined with its association with the young LMC supernova remnant N49 (e.g. Cline 1982), suggests that this source is rapidly spinning down. Spindown from a much shorter period, in the age $t_{0526-66}$ of N49, corresponds to a polar dipole field of $\sim 6 \times 10^{14} (t_{0526-66}/10^4 \text{ yr})^{-1/2}$ G if the classical magnetic dipole formula applies (DT92). Although rotational modulation of the persistent emission of SGR 0526-66 has not yet been detected with compelling statistical confidence (Kulkarni et al. 2000), two other sources SGR 1806-20 and SGR 1900+14 are observed to spin down rapidly (Kouveliotou et al. 1998b, 1999).

The observed \dot{P} variability of these stars (Woods et al. 1999; 2000) may be surprising at first sight, if they are identified as isolated, non-accreting neutron stars. However, as we have argued in detail in this paper, the bright X-ray outbursts provide direct evidence for sudden deformations of the external magnetic field in the SGR sources. The rate of spindown of an isolated neutron star is controlled by the electrical current flowing across its speed-of-light cylinder. Variations in the external magnetic field will, therefore, cause a *modulation* of the spindown torque – either through a large-scale twisting of the external magnetic field (Thompson et al. 2001); or through a magnetically-powered wind (Thompson & Blaes 1988; Thompson et al. 2000). The wind model requires dipole fields $\gtrsim 1 \times 10^{14}$ G for the SGRs with measured spindown, unless the energy in a wind exceeds the *observed*

X-ray output by more than an order of magnitude.

Note that several radiopulsars with spindown fields $B_{dipole} > B_{QED}$ have recently been found. The present record value of B_{dipole} inferred from P and \dot{P} in a radiopulsar is 1.1×10^{14} G (polar field) for PSR 1814-1744 (Camilo et al. 2000). This means that *the minimum magnetic moment which we have inferred from the flare physics is near the upper end of the range measured in radio pulsars*. The dipole field of PSR 1814-1744 is a factor 10 – 20 weaker than that inferred from the spindown of SGRs 1806-20 and 1900+14 if the magnetic dipole formula applies; but can plausibly be reduced by a factor of 3 – 10 in the presence of persistent currents (Kouveliotou et al. 1998b, 1999; Harding, Contopoulos, & Kazanas 1999; Thompson et al. 2000, 2001).

On the other hand, PSR 1814-1744 sits close in the $P - \dot{P}$ plane to the magnetar candidate AXP 1E2259+586. Nonetheless, the spindown age of 1E 2259+586 exceeds by a factor $\sim 10 - 30$ the age of the surrounding supernova remnant CTB 109 (e.g. Kaspi, Chakrabarty, & Steinberger 1999). Given the rapid spindown observed in the other SGR and AXP sources, this suggests that the spindown torque of 1E 2259+586 has decayed by a factor ~ 10 from its historic average. Note that the interior, toroidal magnetic fields of radiopulsars could be much weaker than those of SGRs and AXPs (TD93), which would provide an explanation for why PSR 1814-1744 is a much weaker X-ray source than the AXPs (Pivovarov, Kaspi, & Gotthelf 2000).

5. The absence of a significant perturbation to the long-term spindown rate of SGR 1900+14 in the few months following the August 27 event, implies only a small change in the external dipole field coinciding with the release of $\sim 10^{44}$ ergs (Woods et al. 1999; Thompson et al. 2000).

6. The detection of extended afterglow from the heated surface of a Soft Gamma Repeater is expected following exposure to a trapped fireball. The amount of fireball energy absorbed by the crust increases linearly with the surface B-field at large magnetic flux densities (TD95). This effect has been observed in some short SGR bursts (Strohmayer & Ibrahim 1998), and has been related to an extended, faint oscillatory tail that was observed in an August 29 outburst from SGR 1900+14 (two days after the August 27 giant flare; Ibrahim et al. 2000).

We thank Marco Feroci and Kevin Hurley for a stimulating collaboration which inspired this work, and Lars Bildsten, Max Lyutikov, George Pavlov, and Mal Ruderman for conversations. We also thank the Institute for Theoretical Physics at the University of California at Santa Barbara (NSF grant PHY99-0749) for its hospitality and support during the completion of this paper. CT acknowledges the support of NASA grant NAG5-3100,

NSERC grant RGPIN 238487-01, and the Alfred P. Sloan Foundation. RD acknowledges support from Texas Advanced Research Project grant no. ARP-028 and NASA grant NAG5-8381.

REFERENCES

- Adler, S.L., 1971, *Ann. Phys.*, 67, 599
- Barat, C., Chambon, G., Hurley, K., Niel, M., Vedrenne, G., Estuline, I.V., Kurt, V.G., and Zenchenko, V.M. 1979, *A&A*79, L24
- Barat, C., Hayles, R.I., Kurley, K., Niel, M., Vedrenne, G., Desai, U., Estulin, I.V., Kurt, V.G., & Zenchenko, V.M. 1983, *A&A*, 126, 400
- Baring, M.G. 1995, *ApJ*, 440, L69
- Baym, G., Pethick, C., Pines, D., & Ruderman M.A. 1969, *Nature*, 224, 872
- Baym, G. & Pines, D. 1971, *Ann. Phys.*, 66, 816
- Berestetskii, V.B., Lifshitz, E.M., & Pitaevskii, L.P. 1980, *Quantum Electrodynamics*, (Oxford: Pergamon Press)
- Blaes, O., Blandford, R.D., Goldreich, P., & Madau P. 1989, *ApJ*, 343, 839
- Camilo, F., Kaspi, V.M., Lyne, A.G., Manchester, R.N., Bell, J.F., D’Amico, N., McKay, N.P.F., & Crawford, F. 2000, *ApJ*, 541, 367
- Cheng, B., Epstein, R.I., Guyer, R.A. & Young, C. 1996, *Nature*, 382, 518
- Cline, T. et al. 1980, *ApJ* 237, L1
- Cline, T. 1982, in *Gamma-ray Transients and Related Astrophysical Phenomena*, ed. R.E. Lingenfelter, H.S. Hudson, & D.M. Worrall (New York: AIP), 17
- Cline, T. et al. 1982, *ApJ* 255, L45
- Dicus, D.A. 1972, *Phys. Rev. D*, 6, 941
- Duncan, R.C. 1998, *ApJ*, 498, L45
- Duncan, R.C. 2000 in *Gamma-Ray Bursts: Fifth Huntsville Symposium*, ed. R.M. Kippen, R.S. Mallozzi, & G.J. Fishman (New York: AIP), 830 ([astro-ph/0002442](#))

- Duncan, R.C. & Thompson, C., 1992, ApJ, 392, L9 (DT92)
- Easson, I. & Pethick, C.J. 1979, ApJ, 227, 995
- Fatuzzo, M. & Melia, F. 1993, ApJ, 408, L9
- Fenimore, E.E., et al., 1996, ApJ, 460, 964
- Feroci, M. et al. 1999, ApJ 515, L9
- Feroci, M., Hurley, K., Duncan, R.C., & Thompson C., ApJ, 549, 1021 (Paper I)
- Frail, D., Kulkarni, S., and Bloom, J., 1999, Nature 398, 127
- Goldreich, P. & Reisenegger A. 1992, ApJ, 395, 250
- Gogus et al. 1999 ApJ, 526, L93
- Gogus et al. 2000 ApJ, 532, L121
- Gotthelf, E.V. & Vasisht, G. 2000, in Pulsar Astronomy – 2000 and Beyond, eds. M. Kramer et al. (ASP Conference Series), p. 699
- Harding, A.K., Contopoulos, I., & Kazanas, D. 1999, ApJ, 525, L125
- Herold, H. 1979, Phys. Rev. D, 19, 2868
- Heyl, J.S. & Kulkarni, S.R. 1998, ApJ, 506, L61
- Hulleman, F., van Kerkwijk, M.H., Verbunt, F.W.M., & Kulkarni, S.R. 2000a, A&A, 358, 605
- Hulleman, F., van Kerkwijk, M.H., & Kulkarni, S.R. 2000b, Nature, 408, 689
- Hurley, K. et al. 1999b, Nature 397, 41
- Hurley, K. et al. 1999a, ApJ, 510, L107
- Hurley, K. et al. 1999c, ApJ, 510, L111
- Hurley, K. et al. 1999d, ApJ 523, L37
- Hurley, K. 2000, in Gamma-Ray Bursts: 5th Huntsville Symposium, ed. R.M. Kippen, R.S. Mallozzi, & G.J. Fishman (New York: AIP), X

- Ibrahim, A.I., Strohmayer, T.E., Woods, P.M., Kouveliotou, C., Thompson, C., Duncan, R.C., Dieters, S., Swank, J.H., van Paradijs, J., & Finger, M. 2000, ApJ, 558, 237
- Kaplan, D.L., Kulkarni, S.R., van Kerkwijk, M.H., Rothschild, R.E., Lingenfelter, R.L., Marsden, D., Danner, R., & Murakami, T. 2001, ApJ, 566, 399
- Kaspi, V. M., Chakrabarty, D., & Steinberger, J. 1999, ApJ, 525, L33
- Kouveliotou, C., et al. 1993, Nature, 362, 728
- Kouveliotou, C. et al. 1998b, IAU Circular no. 6929, June 3, 1998
- Kouveliotou, C., et al., 1998a, Nature 393, 235
- Kouveliotou et al. 1999, ApJ, 510, L115
- Kudari, A. 1997, Master's Thesis, University of Texas at Austin
- Kulkarni, S.R., et al., preprint
- Lattimer, J.M. & Mazurek, T.J. 1981, ApJ, 246, 955
- Lindblom, L. & Detweiler, S.L. 1983, ApJS, 53, 73
- Lorenz, C.P., Ravenhall, D.J., & Pethick C.J. 1993, Phys. Rev. Lett. 70, 379
- Lynden-Bell, D. & Boily, C. 1994, MNRAS, 267, 146
- Mazets, E.P., Golenetskii, S.V., and Gur'yan, Yu.A. 1979a, Soviet Astron. Lett., 5(No.6),343
- Mazets, E.P., et al., 1979b, Nature, 282, 587
- Mazets, E.P., Cline, T.L., Aptekar', R.L., Butterworth, P.S., Frederiks, D.D., Golenetskii, S.V., Il'Inskii, V.N., & Pal'Shin, V.D. 1999, Astron. Lett., 25, 635
- Melia, F. & Fatuzzo, M. 1995, ApJ, 438, 904
- Mészáros, P. 1992, High Energy Radiation from Magnetized Neutron Stars (Chicago: University Press).
- Mijic & Linker 1994, ApJ 430, 898
- Miller, M.C. 1995, ApJ, 448, L29
- Murakami, T.. et al., 1994, Nature, 368, 127

- Murakami, T. et al. 1999, *ApJ*, 510, L119
- Negele, J.W. & Vautherin, D. 1973, *Nuc. Phys.*, A207, 298
- Ogata, S. & Ichimaru, S. 1990, *Phys. Rev. A*, 42, 4687
- Paczynski, B., 1992, *Acta Astron.*, 42, 145
- Palmer, D.M. 1999, *ApJ*, 512, L113
- Pendleton, G.N., Paciasas, W.S., Briggs, M.S., Preece, R.D., Mallozzi, R.S., Meegan, C.A., Horack, J.M., Fishman, G.J., Band, D.L., Matteson, J.L., Skelton, R.T., Hakkila, J., Ford, L.A., Kouveliotou, C., Koshut, T.M. 1997, *ApJ*489, 175
- Perna, R., Hernquist, L., & Narayan R. 2000, *ApJ*, 541, 344
- Pethick, C.J. & Potekhin, A.Y. 1998, *Phys. Lett.*, B427, 7
- Pivovarov, M.J., Kaspi, V.M., & Gotthelf, E.V. 2000, *ApJ*, 528, 436
- Ramaty, R., Bonazzola, S., Cline, T.L., Kazanas, D., Mészáros, P., & Lingenfelter, R.E. 1980, *Nature*, 287, 122
- Reisenegger, A. & Goldreich P. 1992, *ApJ*, 395, 240
- Ruderman, M. 1991, *ApJ*, 382, 576
- Schinder, P.J., Schramm, D.N., Wiita, P.J., Margolis, S.H., & Tubbs, D.I. 1987, *ApJ*, 313, 531
- Silant'ev, N.A. & Iakovlev, D.G. 1980, *Ap& SS*, 71, 45
- Strohmayer et al. 1991, *ApJ*, 375, 679
- Strohmayer, T.E. & Ibrahim, A. 1998, in *Gamma-Ray Bursts: 4th Huntsville Symposium*, ed. C.A. Meegan, R.D. Preece, & T.M. Koshut (New York: AIP), p. 947
- Thompson 1997, in ‘*Relativistic Jets in AGN*’, ed. M. Ostrowski, M. Sikora, G. Madejski, & M.C. Begelman, Cracow, p. 63
- Thompson, C. 2000, in *The Neutron Star-Black Hole Connection*, ed. V. Connaughton, C. Kouveliotou, J. van Paradijs, & J. Ventura (Dordrecht: Reidel), in press
- Thompson, C. & Blaes, O. 1998, *Phys. Rev. D*, 57, 3219

- Thompson, C. & Duncan R.C. 1992, in Compton Gamma Ray Observatory, ed. M. Friedlander, N. Gehrels, & R.J. Macomb (New York: AIP), p. 1085
- Thompson, C. & Duncan, R.C. 1993, ApJ, 408, 194 (TD93)
- Thompson, C.& Duncan, R.C., 1995, MNRAS, 275, 255 (TD95)
- Thompson, C. & Duncan, R.C. 1996, ApJ, 473, 322 (TD96)
- Thompson, C., Duncan, R.C., Woods, P.M., Kouveliotou, C., Finger, M.H., & van Paradijs, J. 2000, ApJ, 543, 340 ([astro-ph/9908096](#))
- Thompson, C., Lyutikov, M., & Kulkarni S.R. 2001, in preparation
- Ulmer, A. 1994, ApJ, 437, L111
- Vasisht, G., et al., 1994, ApJ, 431, L35
- Woods, P.M., Kouveliotou, C., van Paradijs, J., Finger, M.H., Thompson, C., Duncan, R.C., Hurley, K., Strohmayer, T., Swank, J., & Murakami, T. 1999, ApJ, 524, L55
- Woods, P., Kouveliotou, C., Gogus, E., Finger, M.H., Swank, J., Smith, D.A., Hurley, K., & Thompson, C., ApJ, ApJ, 552, 748

Table 1. Fireball Indices

Dimensions D_c	Energy Density $U \propto T^{\mu_1} B^{\mu_2}$		Flux $F \propto T^{\sigma_1} B^{\sigma_2}$		Fireball Structure $T \propto r^\gamma \quad B \propto r^\beta$	
	μ_1	μ_2	σ_1	σ_2	γ	β
1	4	0	5/2	0	-1	*
1	4	0	0	4/3	-1/6	0
1	4	0	0	4/3	0	3/8
1	2	1	3/2	1	*	2
1	2	1	0	4/3	-1/3	0
1	2	1	0	4/3	0	6/7
2	4	0	5/2	0	-1/2	*
2	4	0	0	4/3	-1/12	0
2	4	0	0	4/3	0	3/16
2	2	1	3/2	1	*	1
2	2	1	0	4/3	-1/6	0
2	2	1	0	4/3	0	3/7

Note. — The last two columns give the values of fireball structure indices needed to explain the observed time-dependence of the August 27 event ($\chi = 3$). The symbol * means that the observed time-evolution is insensitive to this index, i.e., any value would work.

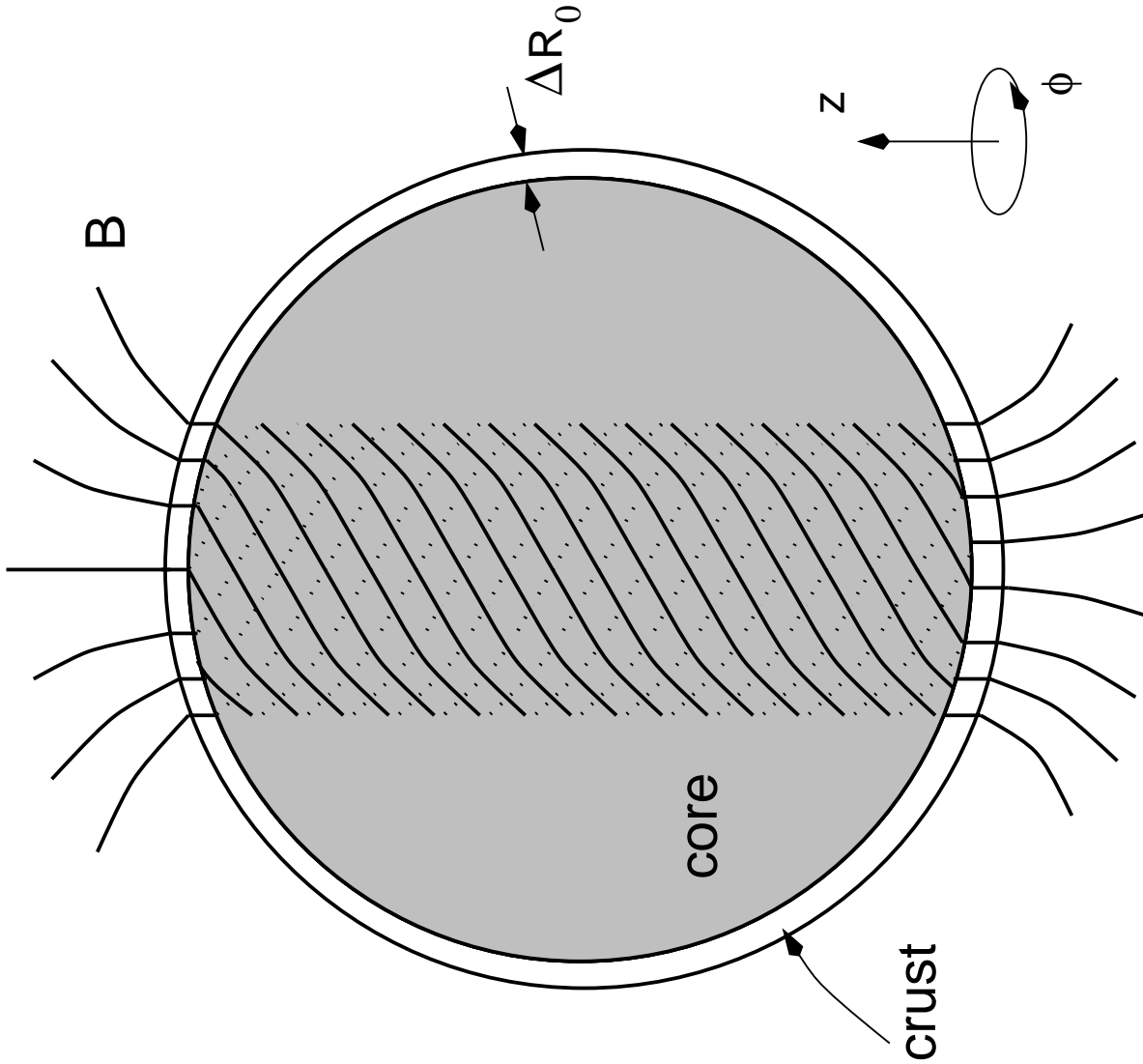


Fig. 1.— An almost spherical star is threaded by a uniform poloidal magnetic field. This field threads both the liquid core and the solid, outer crust of the star. In the core, the field is twisted, creating a toroidal component.

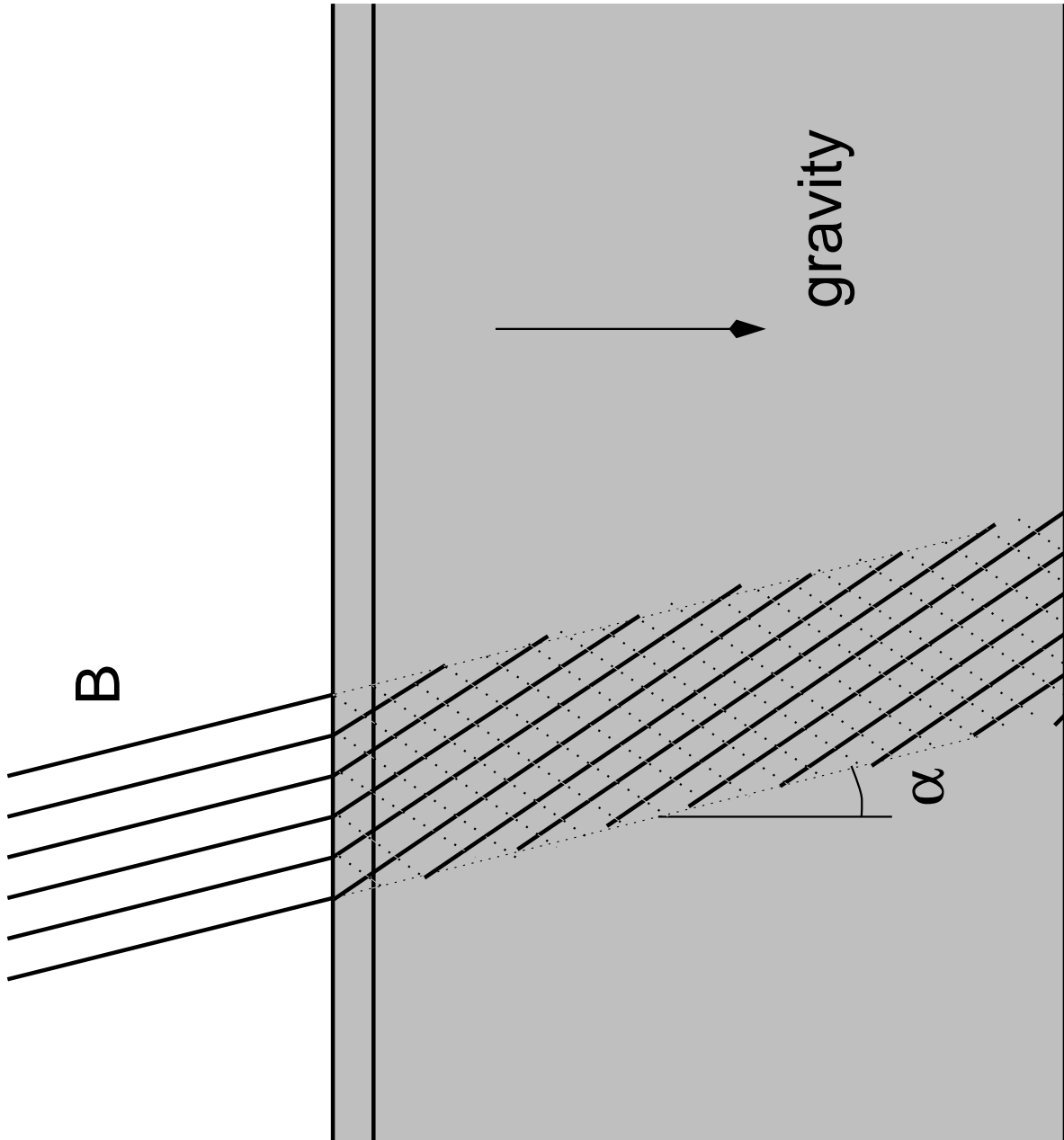


Fig. 2a.— A twisted bundle of magnetic flux threads a conducting medium, which is stratified along planes which run perpendicular to the direction of gravity. The flux bundle is tilted by angle α with respect to gravity; it may be anchored from above and below.

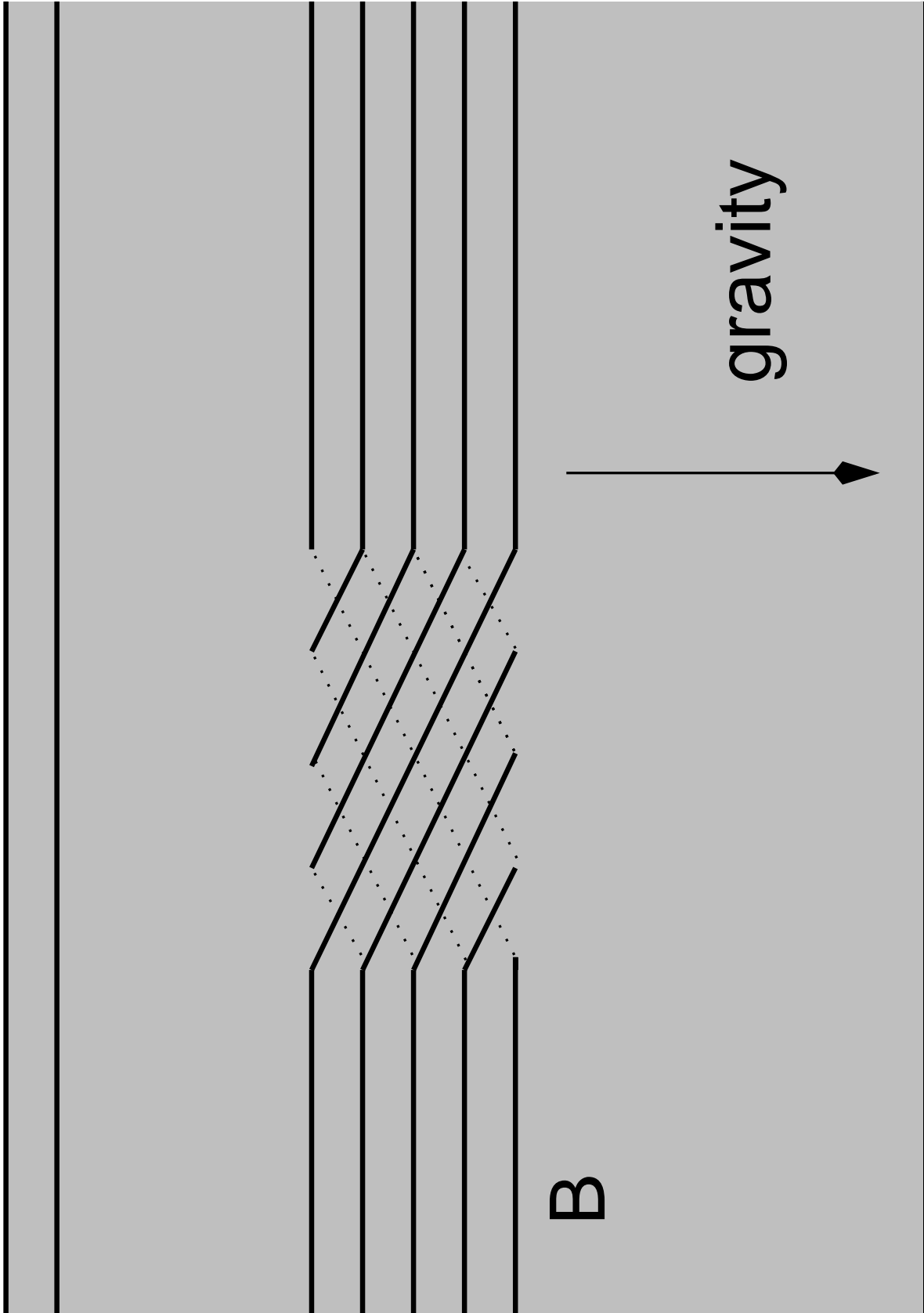


Fig. 2b.— When the flux bundle runs perpendicular to the direction of stratification, a localized twist is prevented from spreading out along the field through purely hydromagnetic

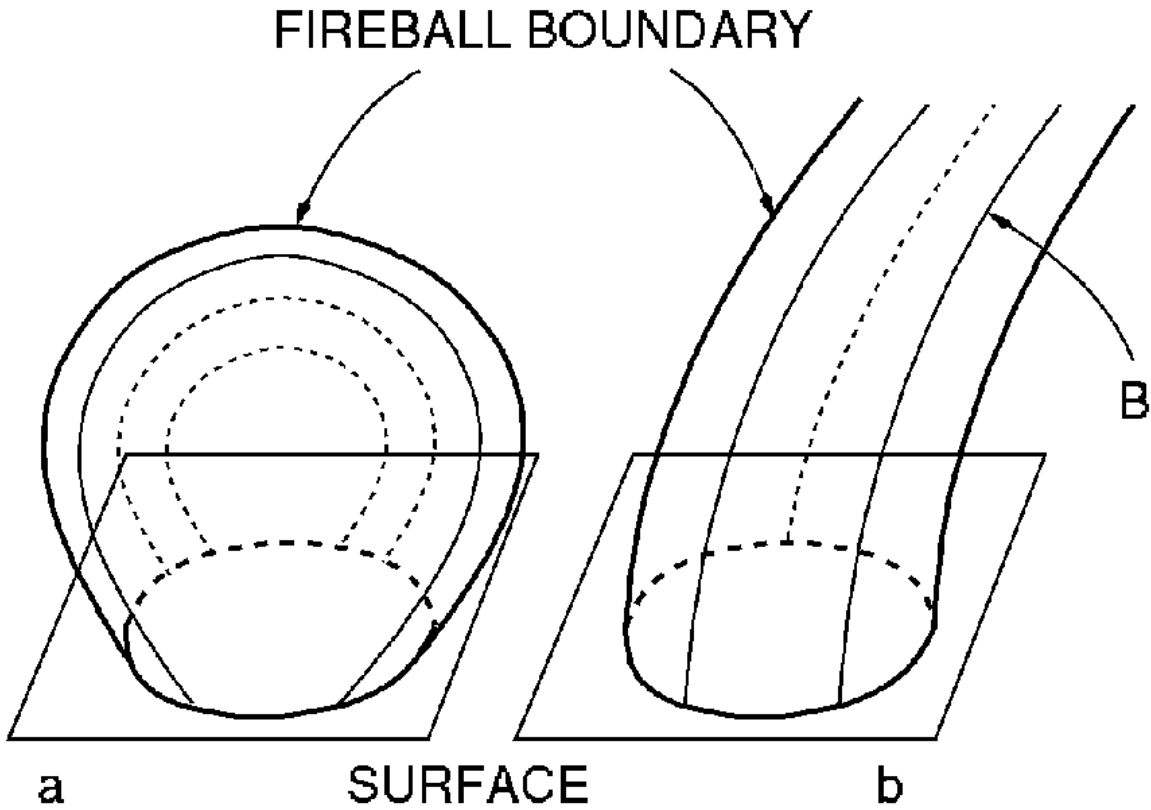


Fig. 3.— A trapped fireball releases energy as its cool outer surface contracts. We illustrate two possible geometries (approximately spherical and cylindrical) for the fireball. The measured fluence of the extended tail of a giant flare, combined with the absence of a measurable perturbation to the light curve from pair neutrino cooling, sets a lower bound to the dipole moment of the confining magnetic field.

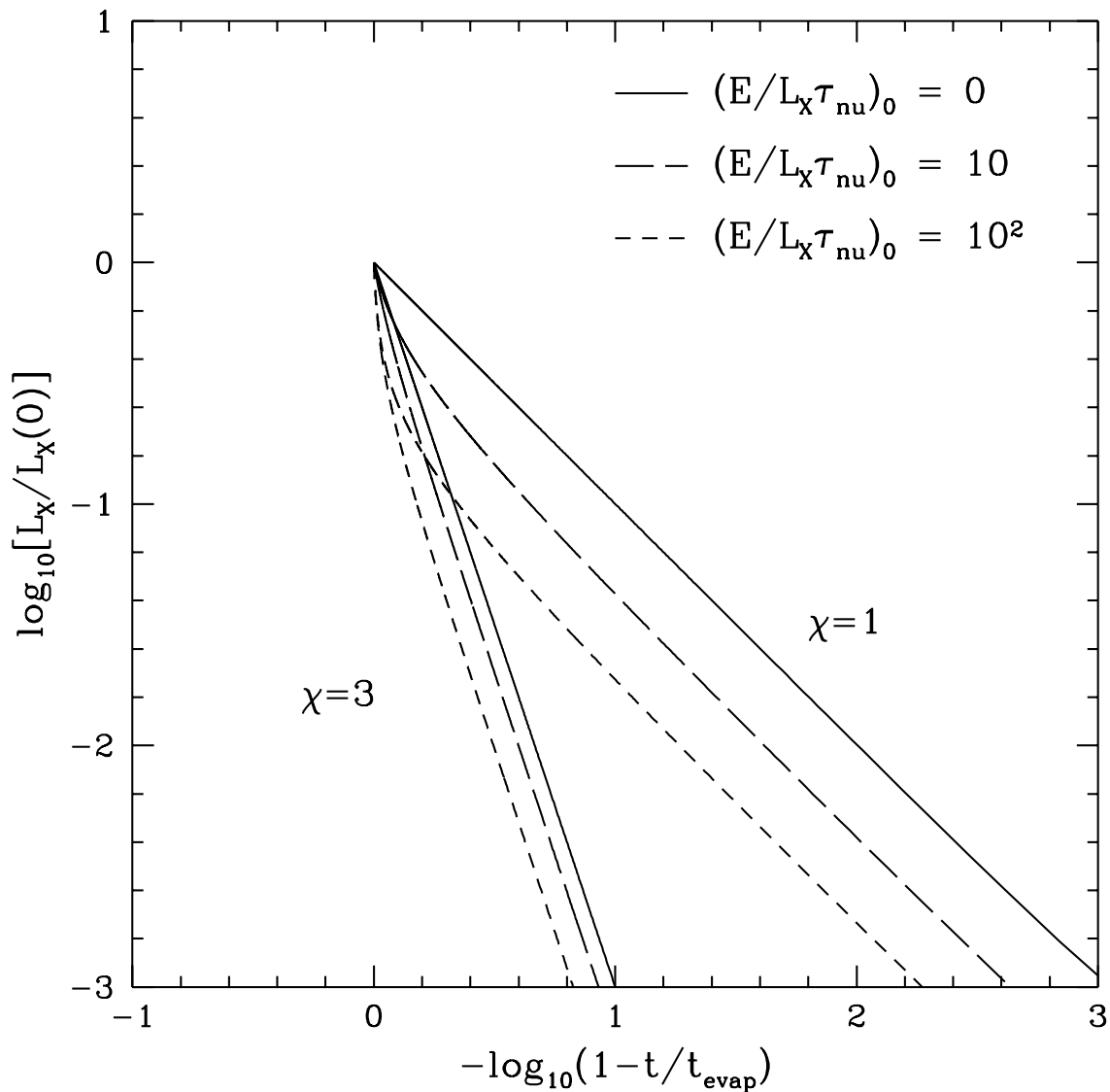


Fig. 4a.— Surface X-ray luminosity of a homogeneous, trapped fireball, whose radiative area scales with the fireball volume as $A \sim V^{0.75}$ ($\chi = 3$; lower curves) and $A \sim V^{0.5}$ ($\chi = 1$; upper curves). Within each set of curves, the solid curve includes no neutrino cooling. The long-dashed and short-dashed curves correspond to uniform pair neutrino cooling, with an initial cooling rate 1 and 10 times the initial surface X-ray luminosity.

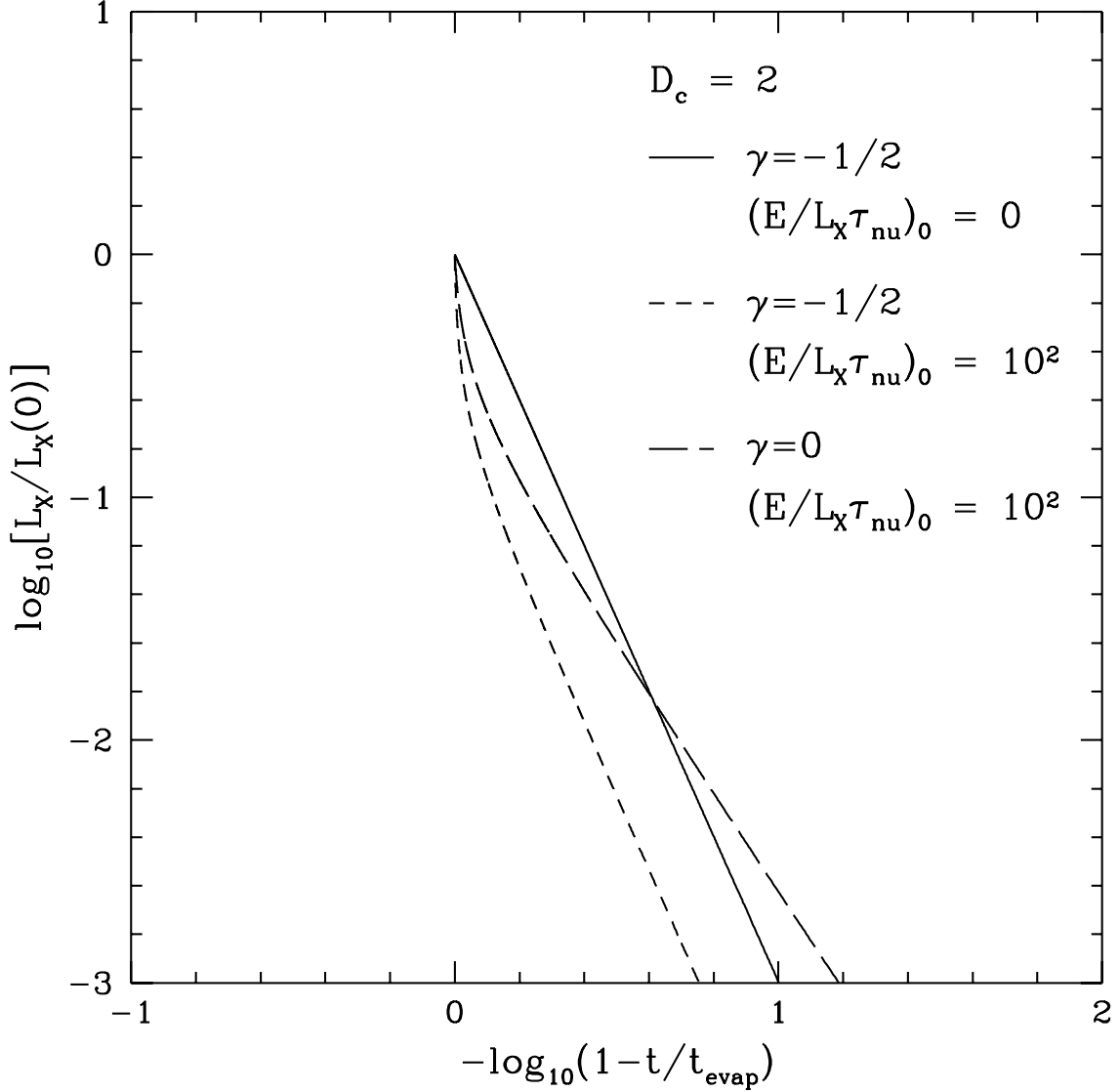


Fig. 4b.— Surface X-ray luminosity of a spherical trapped fireball ($D_c = 2$), showing the effects of neutrino cooling on the shape of the lightcurve. The bold curve ($\chi = 3$) closely approximates the observed lightcurve of the August 27 flare. In a homogeneous magnetic field, this fireball index corresponds to a mild temperature gradient $\gamma = -\frac{1}{2}$. The short-dashed curve describes the effect of pair-neutrino cooling on the X-ray lightcurve, with the neutrino luminosity initially 100 times the cooling X-ray luminosity. The same relative neutrino cooling rate, but a different temperature structure ($\gamma = 0$), brings closer agreement with the observed light curve, but there remains some difference in shape (long-dashed curve).

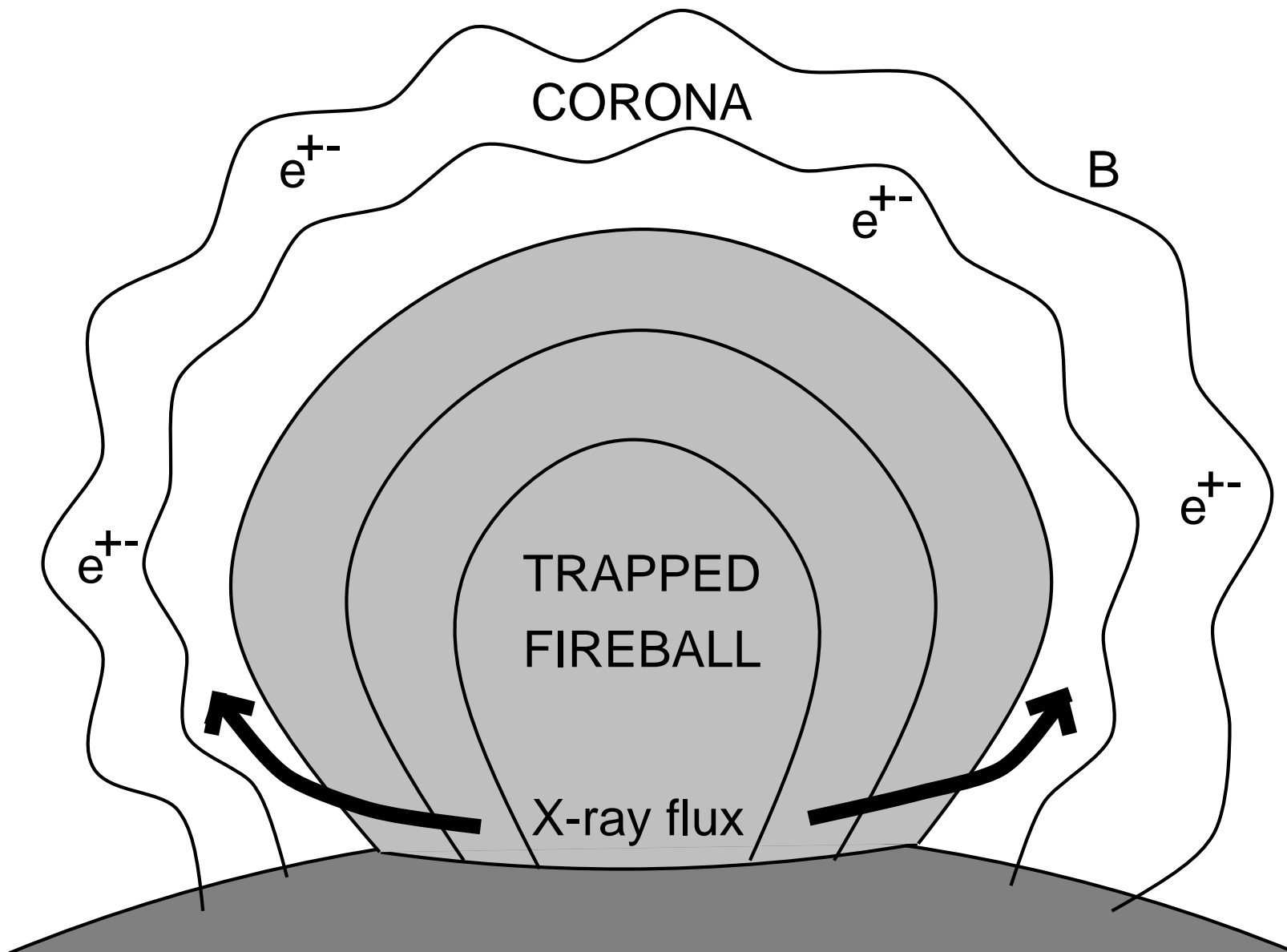


Fig. 5.— A persistent seismic excitation of the neutron star crust will in turn excite sheared (current-carrying) Alfvén waves on extended magnetic field lines in the star’s magnetosphere. Non-linear couplings between these trapped Alfvén modes generate a turbulent cascade that creates a hot corona. At the high luminosity (and inferred compactness) of the August 27 smooth tail, this corona consists of electron-positron pairs with only a slightly higher temperature than the X-ray photons (which are assumed to have a Wien distribution). The dominant source of fresh Compton seeds for this Corona could either be provided by an interior trapped fireball (as depicted); or, alternatively, by photon splitting.

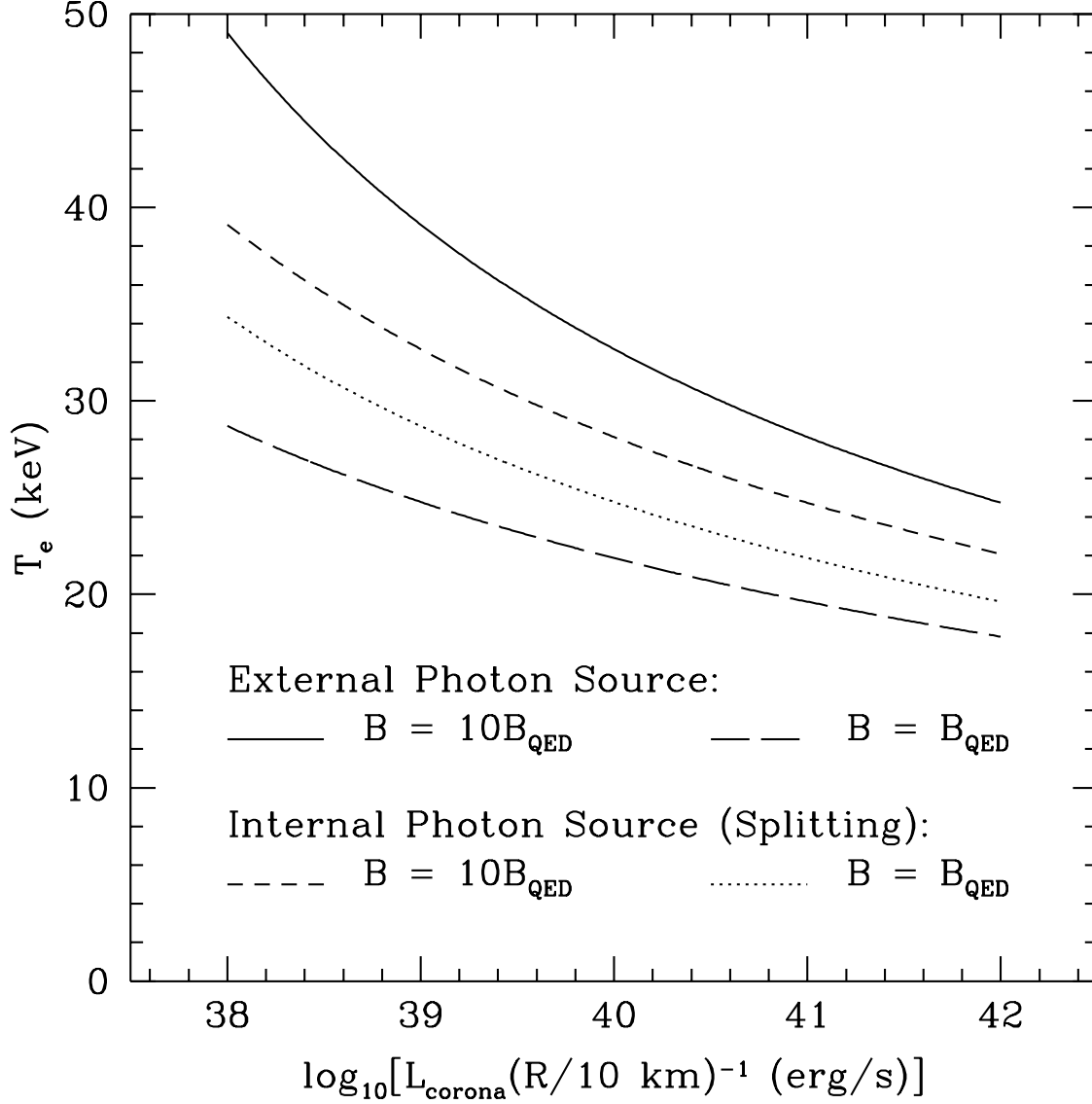


Fig. 6.— Equilibrium temperature of a electron-positron corona (of size R), under two different assumptions about the mechanisms of photon creation and radiative cooling. The top and bottom curves correspond to an external source of (E-mode) photons (eq. [77]). The second set of curves corresponds to an internal photon source, which is balanced by outward diffusion through the O-mode (eq. [79]). The maximum coronal luminosity, above which no stable balance between heating and cooling is possible, lies close to $\sim 10^{42}$ erg s $^{-1}$ (eqs. [82] and [89]).

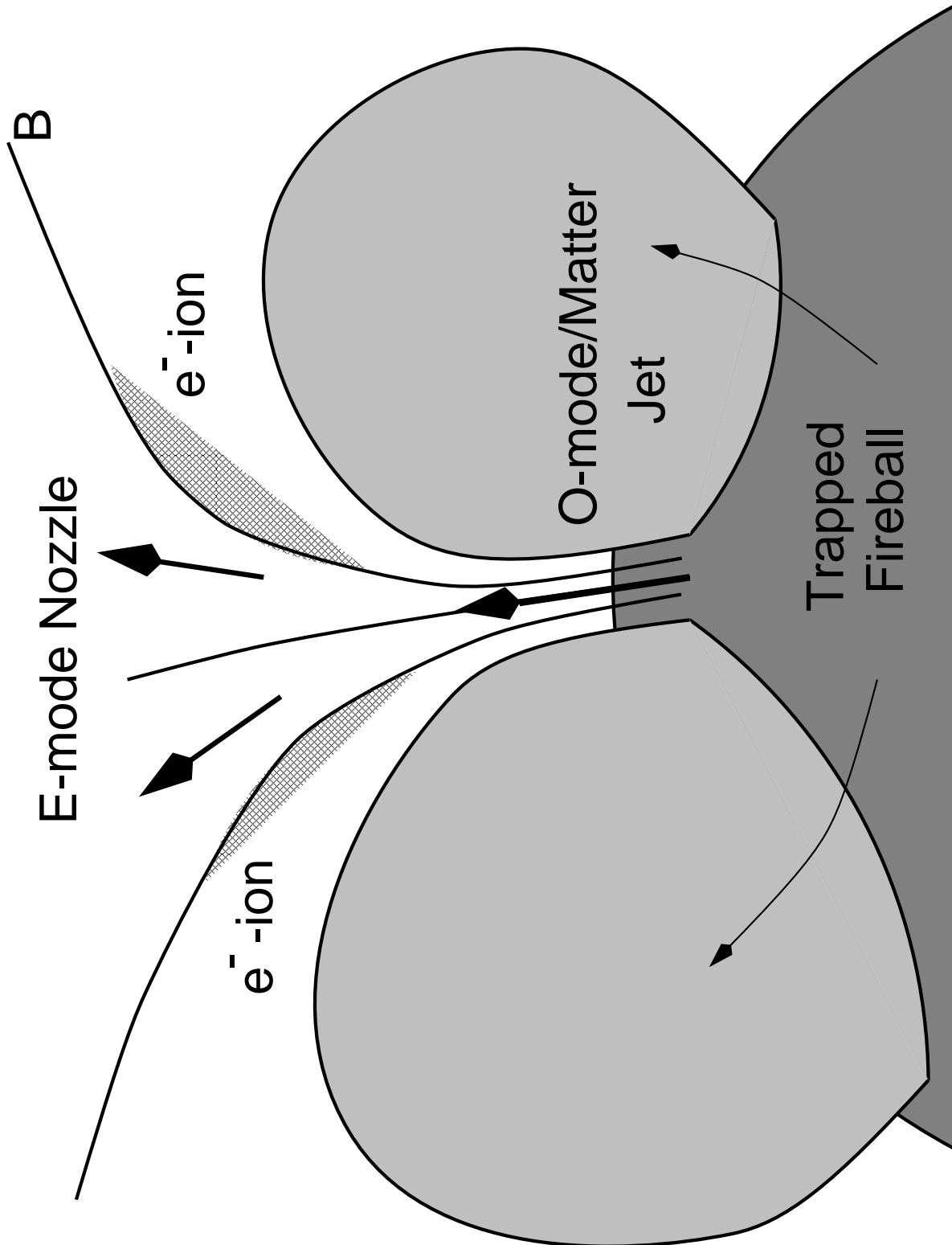


Fig. 7.— A trapped fireball releases energy as its cool outer surface contracts. The radiative flux across the fireball surface is concentrated close to the surface of the neutron star, where the E-mode scattering opacity is most strongly suppressed by the intense magnetic field. A collimated flux of both the O-mode and E-mode radiation can be generated along more extended magnetic field lines. The O-mode couples tightly to the electrons near the stellar surface, even if a small fraction of the hyper-Eddington radiative flux is carried by matter:

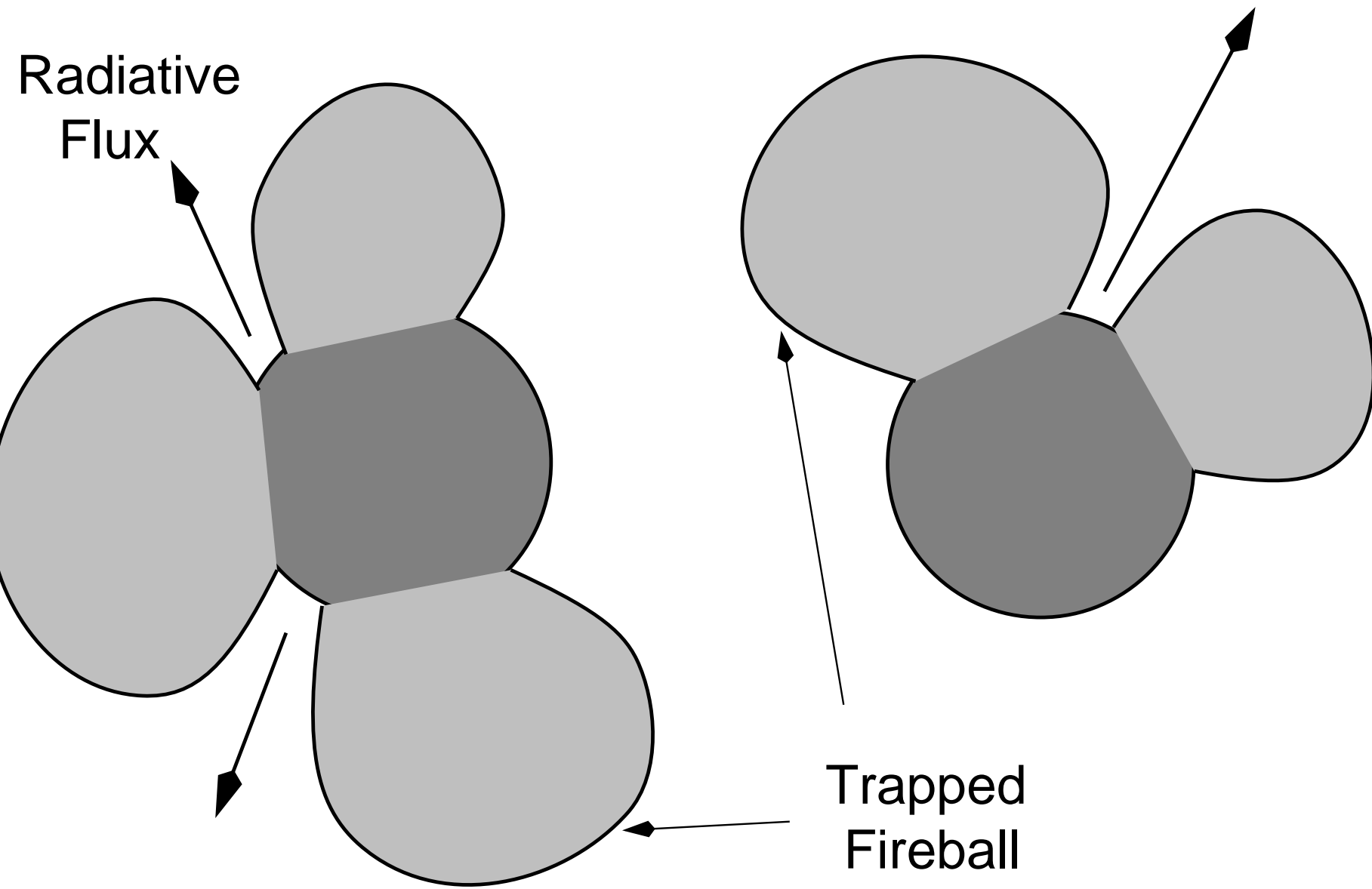


Fig. 7.— A geometry is suggested both for the August 27 giant flare from SGR 1900+14 (left; four sub-pulses) as well as the original March 5 flare from SGR 0525-66 (right; two sub-pulses). Each large arrow denotes a fan beam of X-rays and outflowing, relativistic matter. The angular velocity of each source is assumed to be oriented so that each fan beam is observed twice per rotation, yielding two sub-pulses per beam. In this model, the burst light curve is sensitive to the configuration of the particular subset of the closed magnetic field lines which confine the hot e^\pm -photon plasma. Thus, the presence of higher multipoles in SGR 0526-66 is not excluded by the observation of two sub-pulses within the tail of the March 5 flare.